










# Genetically encoded intrabody probes for labeling and manipulating AMPA-type glutamate receptors

Received: 27 July 2023

Accepted: 14 November 2024

Published online: 29 November 2024

 Check for updates

Dean J. Kareemo , Christina S. Winborn, Samantha S. Olah, Carley N. Miller , JungMin Kim , Chelsie A. Kadgien , Hannah S. Actor-Engel, Harrison J. Ramsay , Austin M. Ramsey , Jason Aoto  & Matthew J. Kennedy  

Tools for visualizing and manipulating protein dynamics in living cells are critical for understanding cellular function. Here we leverage recently available monoclonal antibody sequences to generate a set of affinity tags for labeling and manipulating AMPA-type glutamate receptors (AMPARs), which mediate nearly all excitatory neurotransmission in the central nervous system. These antibodies can be produced from heterologous cells for exogenous labeling applications or directly expressed in living neurons as intrabodies, where they bind their epitopes in the endoplasmic reticulum and co-traffic to the cell surface for visualization with cell impermeant fluorescent dyes. We show these reagents do not perturb AMPAR trafficking, function, mobility, or synaptic recruitment during plasticity and therefore can be used as probes for monitoring endogenous receptors in living neurons. We also adapt these reagents to deplete AMPARs from the cell surface by trapping them in the endoplasmic reticulum, providing a simple approach for loss of excitatory neurotransmission. The strategies outlined here serve as a template for generating similar reagents targeting diverse proteins as more antibody sequences become available.

Tools for visualizing and manipulating cellular proteins are cornerstones of experimental biology. Traditional approaches for labeling proteins in cells and tissue generally rely on antibody staining and visualization with fluorescent or chromogenic compounds. Requiring fixation and permeabilization, these approaches are not compatible with imaging proteins in live cells. Recent advances in gene editing overcome this limitation by allowing direct fusion of fluorescent probes to endogenous proteins<sup>1–5</sup>, but these approaches can be challenging to implement in primary non-dividing cells, have the potential for disruption of the gene under investigation, and can be difficult to multiplex with additional genetic toolsets. For protein manipulation, genetic knockout strategies are the gold standard, but generally lack

temporal precision, are irreversible and can result in compensatory alterations. Moreover, generating animals with multiple gene manipulations can be time-consuming and expensive.

To overcome these issues, genetically encoded affinity probes are starting to emerge for both labeling and manipulating endogenous proteins in live cells. For example, fibronectin intrabodies generated with mRNA display (FingRs) have been developed for a small number of synaptic proteins, allowing their direct visualization and targeted ablation in live cells<sup>6–8</sup>. Likewise, single-chain camelid antibodies have been sequenced and adapted as genetically expressed probes for common epitope tags and fluorescent proteins<sup>9,10</sup>. Finally, monoclonal antibody sequences are becoming increasingly available, offering the

Department of Pharmacology, University of Colorado School of Medicine, Anschutz Medical Campus, Aurora, CO 80045, USA.

✉ e-mail: [matthew.kennedy@cuanschutz.edu](mailto:matthew.kennedy@cuanschutz.edu)

potential for new genetically encoded affinity reagents for visualizing and manipulating a broad host of proteins in living cells<sup>11–13</sup>.

Here we leveraged recently available sequences of monoclonal antibodies against ionotropic AMPA-type glutamate receptors (AMPARs)<sup>14</sup>, which mediate most fast excitatory neurotransmission in the central nervous system, to generate a set of recombinant monoclonal antibodies (R-mAbs) for labeling endogenous AMPARs and manipulating their trafficking in live neurons. AMPAR R-mAbs can be expressed in heterologous cells as HaloTag<sup>15</sup> fusions and collected from the culture media for AMPAR labeling on live cells with the palette of bright and photostable HaloDye ligands<sup>16,17</sup>. R-mAbs can also be genetically expressed directly in neurons as intrabodies (i-mAbs), where they bind their respective epitopes in the endoplasmic reticulum (ER) and co-traffic to the cell surface, allowing their visualization and quantification as they traffic to synapses. In addition to AMPAR labeling, we have adapted i-mAbs for controlling AMPAR exit from the ER, providing a simple approach for blocking excitatory neurotransmission in targeted cell types. We expect these strategies will be generally adaptable to diverse receptors, channels, adhesion proteins and other membrane proteins and secreted factors as monoclonal antibody sequences become increasingly available.

## Results

### Validating AMPA receptor labeling reagents derived from monoclonal antibodies

AMPARs are tetrameric assemblies of GluA1–4 subunits<sup>18</sup>. To develop AMPAR probes, we used previously reported sequences of monoclonal antibodies against the GluA1 and GluA2 subunits<sup>14</sup>, which are expressed throughout the central nervous system<sup>19,20</sup>. There are several issues with using whole IgG antibodies to visualize surface receptors on live cells, notably their multi-valency (i.e., each antibody can bind multiple targets) and large size (~150 kDa), which can lead to receptor cross-linking and disrupted mobility and/or localization<sup>21,22</sup>. Thus, we generated plasmid vectors to express the heavy and light chains (HC and LC) of the previously reported anti-GluA2 Fab fragment (A2 Fab) and single chain variable fragment against GluA1 (A1 scFv)<sup>14</sup>. While R-mAbs could be directly conjugated with fluorescent dyes<sup>23</sup>, we appended a HaloTag<sup>15</sup> to the C-termini of the A1 scFv (A1 scFv-Halo) and the A2 Fab heavy chain (A2 Fab-Halo), allowing us the flexibility of direct and stoichiometric labeling with the expansive palette of bright and photostable HaloDye ligands<sup>17</sup>. Plasmids were transfected into HEK293T cells, with secreted R-mAbs collected from the culture media 3–4 days later and concentrated (Fig. 1a). We confirmed AMPAR binding by adding R-mAb conditioned media to HEK293T cells transfected with plasmids encoding GFP-tagged GluA1 and GluA2 AMPAR subunits or control cells transfected with GFP fill, followed by application of HaloDye (JF635i). Only cells transfected with the AMPAR subunits were labeled (Fig. 1b,c). We further confirmed the specificity of A1 scFv-Halo and A2 Fab-Halo in cultured hippocampal neurons, using CRISPR/Cas9 to disrupt the *GRIA1* and *GRIA2* genes<sup>24</sup>. While robust GluA1 and GluA2 labeling was observed in control cells (expressing Cas9 but no guide RNA), the signal was nearly undetectable in neurons expressing guide RNAs against GluA1 or GluA2, respectively (Fig. 1d,e). We also tested whether A1 scFv-Halo, A2 Fab-Halo, and an scFv we generated from the A2 Fab sequence (A2 scFv-Halo) label AMPARs with similar efficiency as conventional GluA1 and GluA2 IgG antibodies. Because R-mAbs directly compete with our conventional IgG antibodies, we could not co-label the same subunit. Since the majority of synaptic AMPARs contain both the GluA1 and GluA2 subunits<sup>19</sup>, we co-labeled AMPARs with a commercially available anti-GluA2 monoclonal IgG, along with A1 scFv-Halo (Fig. 1f). In separate cells, we labeled with a custom rabbit polyclonal anti-GluA1 IgG<sup>25,26</sup> along with A2 Fab-Halo or A2 scFv-Halo. We also immunostained for Homer1 to identify excitatory synapses. Nearly every synapse labeled by conventional A1 or A2 IgG staining was also positive for the partnering subunit R-mAb signal (A2 IgG with A1

scFv-Halo  $95.26 \pm 3.4\%$ ,  $n = 4016$  synapses from 10 neurons; A1 IgG with A2 Fab  $95.52 \pm 2.0\%$ ,  $n = 4022$  synapses from 9 neurons; A1 IgG with A2 scFv  $98.69 \pm 0.8\%$ ,  $n = 4954$  synapses from 13 neurons). Together these data show recombinantly generated, HaloTag-fused GluA1 and GluA2 R-mAbs can be easily produced and bind selectively and efficiently to neuronal AMPARs.

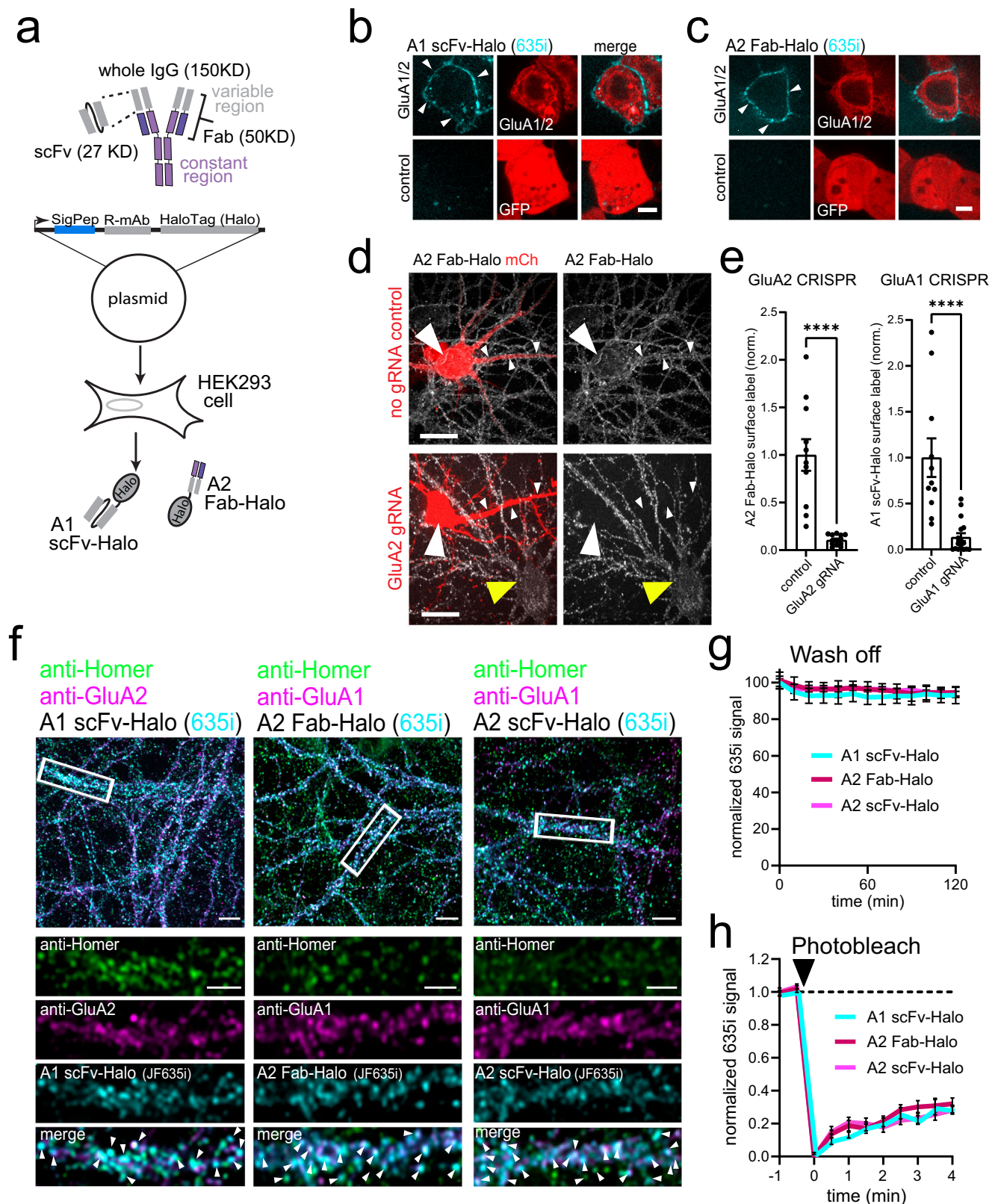
For applications involving longitudinal live imaging experiments, it is necessary that the R-mAbs remain stably bound to their target AMPAR subunits. Thus, we characterized the stability of the interactions by applying R-mAbs to dissociated hippocampal neurons, along with JF635i, then washing out the excess dye/R-mab and imaging every 10 min for 2 h. Following 2 h, we observed  $93.1 \pm 4.7\%$ ,  $94.6 \pm 2.8\%$ , and  $93.9 \pm 1.3\%$  of the baseline signal remained for A2 Fab-halo, A2 scFv-Halo, and A1 scFv-Halo, respectively (Fig. 1g). We also assessed whether surface AMPARs labeled with R-mAbs could laterally diffuse in the membrane by performing fluorescence recovery after photobleaching (FRAP) measurements. Spine-localized AMPARs labeled with A1 scFv-Halo, A2-Fab-Halo and A2-scFv-Halo exhibited comparable levels of recovery (~30%) 5 min following photobleaching (Fig. 1h). While some previous studies using overexpressed AMPARs report larger mobile fractions, ranging from ~80 to 100%<sup>27</sup>, our data more closely agree with recent studies visualizing endogenous AMPARs, either biotinylated and labeled with monomeric neutravidin<sup>28</sup> or using CRISPR approaches to knock in fluorescent tags<sup>5</sup>. Together these experiments show our Halo-tagged A1 and A2 R-mAbs can be used to visualize surface AMPARs on live cells without impeding their mobility.

### Functional characterization of AMPAR R-mAbs

An important consideration for any live cell probe is whether it influences the function and/or localization of its target protein. We first tested basal AMPAR function using whole-cell patch clamp electrophysiology in dissociated hippocampal neurons before and after acute R-mAb application. We observed no significant difference in mEPSC frequency or amplitude when comparing baseline values to values recorded from the same cell 5–7 min following the application of A1 scFv-Halo or A2 Fab-Halo (Fig. 2a,b). We also tested longer-term exposure (30–45 min) to A1 and A2 R-mAbs. Here we compared populations of neurons pre-labeled with R-mAbs to control cells treated with vehicle, containing only HaloDye JF635i (Fig. 2c–f). We intentionally targeted cells with strong R-mAb labeling for whole cell patch clamp recording (examples in Fig. 2c). Once more, we observed no differences in mEPSC amplitude, frequency or kinetics in R-mAb bound cells compared to control cells treated with vehicle only (Fig. 2d–f and Fig. S1).

One of the central mechanisms for learning-related forms of plasticity, such as long-term potentiation (LTP), is the regulated accumulation of surface AMPARs at the postsynaptic membrane<sup>22</sup>. To test if R-mAb bound AMPARs could traffic to synapses following LTP induction, we pre-conjugated A2 Fab-Halo with JF549i and added it to dissociated hippocampal cultures infected with an AAV encoding GFP to visualize cellular morphology. We triggered chemical LTP (cLTP) with an established protocol previously shown to drive accumulation of overexpressed AMPARs at the postsynaptic membrane of a subset of dendritic spines (typically 30–40%)<sup>29,30</sup>. Following cLTP induction in the presence of A2 Fab-Halo, we observed robust growth (structural plasticity) of a similar percentage of dendritic spines compared to unlabeled control cells (persistent growth greater than 1.1-fold, measured 25 min following cLTP onset: control,  $37.1 \pm 2.6\%$  of spines,  $n = 128$  spines from 5 neurons; A2 Fab-Halo  $36.9 \pm 2.3\%$  of spines grew,  $n = 279$  spines from 6 neurons). We also observed a striking enrichment of A2 Fab-Halo bound AMPARs at spines undergoing structural plasticity (Fig. 3a–c). Thus, even our largest R-mAb (A2 Fab-Halo) does not prevent plasticity-induced AMPAR spine accumulation.

While R-mAb labeled AMPARs can traffic to spines following cLTP, we also wanted to test whether they can be activated to support



functional LTP. Here we used whole cell voltage clamp recordings to test whether R-mAbs interfere with LTP in acute hippocampal brain slices cut from P22-28 mice. To ensure deeper penetration of R-mAb into the slices, we used A1 scFv-Halo, which is much smaller than the A2 Fab-Halo used in the dissociated culture experiments. Slices were incubated for at least 90 min with A1 scFv-Halo (pre-conjugated to JF635i) immediately prior to LTP recordings from CA1 pyramidal

neurons. LTP was triggered by pairing 0 mV depolarization with 2 Hz stimulation for 90 sec, which elicited strongly potentiated EPSCs in both control and A1 scFv-Halo treated slices. LTP magnitude, measured as fold-increase in EPSC amplitude 30 min following induction, was indistinguishable between control and A1 scFv-Halo treated slices (Fig. 3d,e). For these experiments we ensured A1 scFv-Halo penetrated to the depth of the recorded cells by filling them with biocytin through

**Fig. 1 | Validating AMPA receptor labeling reagents derived from monoclonal antibodies.** **a** Approach for generating R-mAbs in HEK cells. **b** A1 scFv-Halo (cyan) binds to HEK cells expressing GFP-tagged GluA1 and GluA2 AMPAR subunits (top panels, 29/32 cells from 1 culture) but not control cells (GFP alone, bottom panels, 0/33 cells from 1 culture). Scale bar is 5  $\mu$ m. **c** A2 Fab-Halo (cyan) binds HEK cells expressing GFP-tagged GluA1 and GluA2 AMPAR subunits (top panels, 27/35 cells from 2 cultures) but not control cells (GFP alone, bottom panels, 0/36 cells from 2 cultures). Scale bar is 5  $\mu$ m. **d** Primary hippocampal neuron expressing saCas9 with a gRNA targeting GluA2 or saCas9 alone (no gRNA control) along with mCherry (red). White arrowheads indicate the transfected neurons, yellow arrowhead indicates a neighboring untransfected neuron. Scale bars are 10  $\mu$ m. **e** Quantification of A2-Fab-Halo (left panel) or A1 scFv-Halo (right panel) labeling in cells expressing saCas9 along with GluA2 or GluA1-targeting gRNA (data are normalized to signal from control cells not expressing gRNA) (GluA2 control  $n = 11$  cells, GluA2 gRNA

$n = 18$  cells from 2 cultures, GluA1 control  $n = 11$  cells, GluA1 gRNA  $n = 17$  cells, from 1 culture, two-tailed Student's  $t$ -test, \*\*\*\* $p < 0.0001$  for both GluA1 and GluA2). **f** Left: Hippocampal neurons labeled with designated R-mAb (cyan), designated AMPAR subunit antibody (magenta) and Homer1 (green). White arrowheads indicate colocalization of R-mAb signal with anti-Homer and respective anti-GluA1 or anti-GluA2 antibody. Scale bars are 10  $\mu$ m; insets are 5  $\mu$ m. **g** Quantification of A1 scFv-Halo (cyan), A2 Fab-Halo (red) and A2 scFv-Halo (magenta) JF635i signal stability, normalized to signal immediately following washout ( $t = 0$ ) (A1 scFv-Halo  $n = 50$  dendritic ROIs from 6 cells, A2 Fab-Halo  $n = 50$  dendrite ROIs from 6 cells, A2 scFv-Halo  $n = 50$  dendrite ROIs from 6 cells). **h** Mobility of AMPARs labeled with designated R-mAb, measured by fluorescence recovery after photobleaching. (A1 scFv-Halo  $n = 21$  spines, A2 Fab-Halo  $n = 22$  spines, A2 scFv-Halo  $n = 18$  spines). Data are presented as mean values  $\pm$  SEM. n.s. not significant. Source data are provided as a Source Data file.

the patch pipette and post-hoc labeling with streptavidin-Alexa488. We observed robust JF635i labeling within the volume surrounding dendrites of filled neurons in slices exposed to A1 scFv-Halo compared to slices not exposed to A1 scFv-Halo but incubated with the same concentration of JF635i (Fig. S2).

### Using GluA1 and GluA2 labeling reagents as genetically expressed intrabodies

Since antibodies are normally produced in the ER lumen, we reasoned our probes, which recognize extracellular N-terminal AMPAR epitopes (i.e. exposed in the ER lumen), could be used as intrabodies by direct genetic expression in neurons (heretofore referred to as intrabody mAbs; i-mAbs) (Fig. 4a). We tested this by transfecting cultured hippocampal neurons with A2 Fab-Halo, A2 scFv-Halo or A1 scFv-Halo along with mCh and PSD95<sub>FingR</sub>-GFP to visualize cell morphology and the postsynaptic density (PSD), respectively. After 2–3 days to allow expression and trafficking of i-mAb-bound AMPARs to synapses, we applied the cell-impermeant HaloDye JF635i. For all reagents, we observed punctate labeling on dendritic spines that colocalized with PSD95<sub>FingR</sub>-GFP (Fig. 4b,c). For A2 Fab-Halo and A2 scFv-Halo, we observed minimal labeling of adjacent cells, suggesting little secretion of free (non-AMPA bound) A2 i-mAbs (Fig. 4b). In contrast, we observed some degree of punctate labeling near to, but not overlapping with A1 scFv-Halo expressing neurons (Fig. S3a) suggesting some A1 scFv-Halo can be secreted to label AMPARs on nearby cells.

To assess the stability of the complexes formed between AMPARs and genetically expressed GluA1 or GluA2 i-mAbs, hippocampal neurons expressing A1 scFv-Halo, A2 Fab-Halo, or A2 scFv-Halo were pulse-labeled with JF635i and imaged every 10 min for 2 h. Following 2 h,  $90.4 \pm 5.4\%$ ,  $92.4 \pm 1.4\%$ , and  $92.2 \pm 1.8\%$  of the baseline signal remained for A1 scFv-Halo, A2 Fab-halo, and A2 scFv-Halo, respectively (Fig. 4d). To determine the extent of receptor internalization over the same timeframe (which could lead to an overestimate of binding stability since internalized label would still appear associated with the cell), we engineered a version of the A1 scFv-Halo with a thrombin cleavage sequence between the scFv and the HaloTag. Addition of extracellular thrombin results in the rapid removal of the HaloTag signal, allowing us to quantify the fraction of receptors remaining at the cell surface. A brief thrombin treatment 2 h following pulse labeling with JF635i resulted in a  $83.7 \pm 1.3\%$  decrease in synaptic signal, indicating the majority of the labeled receptors remain on the cell surface, consistent with relatively slow basal AMPAR internalization rates previously reported<sup>31</sup> (Fig. S3b–d).

We were careful to perform the experiments described above in cells with low to moderate i-mAb expression levels because we often observed strong AMPAR mislocalization to the cell body in cells highly overexpressing A1 and A2 scFv-Halo i-mAbs. For example, compared to control cells, we observed a much higher soma-to-dendrite ratio of total GluA1 signal (detected with an intracellular, C-terminal antibody to avoid epitope competition with i-mAbs) in cells transfected with a

high amount (200 ng) of A1 scFv-Halo plasmid, with much of the somatic signal confined to the ER-derived nuclear envelope (Fig. S4a,b). This issue could be resolved simply by transfecting less plasmid (typically 50 ng), which generally yielded lower expression levels, consistent with a previous study showing that some scFv sequences are prone to aggregate at high concentrations<sup>32</sup>. To better resolve this issue, we generated adeno-associated viruses (AAVs) encoding A1 and A2 scFv-Halo sequences under the control of a weaker, neuron-specific promoter (human synapsin). AAV gene delivery generally results in lower and less variable expression levels compared with plasmid-based transfection. Indeed, we observed robust synaptic AMPAR labeling in AAV-infected cells, with a total GluA1 soma-to-dendrite ratio that was indistinguishable from uninfected controls (Fig. S4a,b).

We next tested whether genetically expressing AMPAR i-mAbs (from transfected plasmids and AAVs) interfered with AMPAR function. We used an antibody heavy chain-Halo from an anti-GluA1 antibody<sup>33</sup> (N355/1), which does not bind GluA1 on its own, as a control for overexpression of an ER-localized antibody-based protein. A1 scFv-Halo did not perturb AMPAR-mediated mEPSC frequency or amplitude when introduced by AAV or transfected plasmid (ensuring moderate expression levels when plasmid transfection was used) (Fig. 4e,f; S5a). In contrast, mEPSC frequency, but not amplitude, was severely reduced (control frequency  $2.37 \pm 0.48$  s<sup>-1</sup>, A2 Fab frequency  $0.45 \pm 0.10$  s<sup>-1</sup>, A2 scFv frequency  $0.64 \pm 0.14$  s<sup>-1</sup>) in cells genetically expressing A2 i-mAbs delivered either by plasmid-based transfection (A2 Fab-Halo and A2 scFv-Halo) or AAV (A2 scFv-Halo) (Fig. 4e,g and Fig. S4c). Thus, genetic expression but not acute application of recombinant A2 Fab/scFv appears to disrupt synaptic AMPAR function and/or localization.

Given that A2 i-mAb reagents disrupted basal synaptic transmission, we focused on further validating A1 scFv-Halo as an intrabody probe by first quantifying AMPAR labeling efficiency. Here we simultaneously labeled surface AMPARs with a conventional IgG antibody against GluA2 in neurons infected for 4 days with A1 scFv-Halo AAV, which was visualized with JF635i. Following fixation, we also immunolabeled cells for Homer1 to identify synapses (Fig. 4h). Compared to uninfected controls, there was no change in the mean surface anti-GluA2 signal, indicating overall AMPAR surface levels remain unperturbed by A1 scFv-Halo expression (Fig. 4i). We also observed that nearly all synapses ( $99.37 \pm 0.3\%$ ,  $n = 2654$  synapses from 27 neurons) with detectable anti-GluA2 IgG signal also contained A1 scFv-Halo (JF635i) signal.

With no detectable effect on AMPAR surface delivery or basal synaptic transmission, we next tested whether A1 scFv-Halo interfered with plasticity-regulated AMPAR trafficking. We first measured whether i-mAb-bound AMPARs could laterally diffuse in the membrane by performing FRAP measurements. Spine-localized AMPARs labeled with A1 scFv-Halo i-mAb exhibited ~25% recovery 10 min following photobleaching (Fig. S4d). We next measured homeostatic scaling following prolonged (24 h) blockade of action potentials and NMDA type

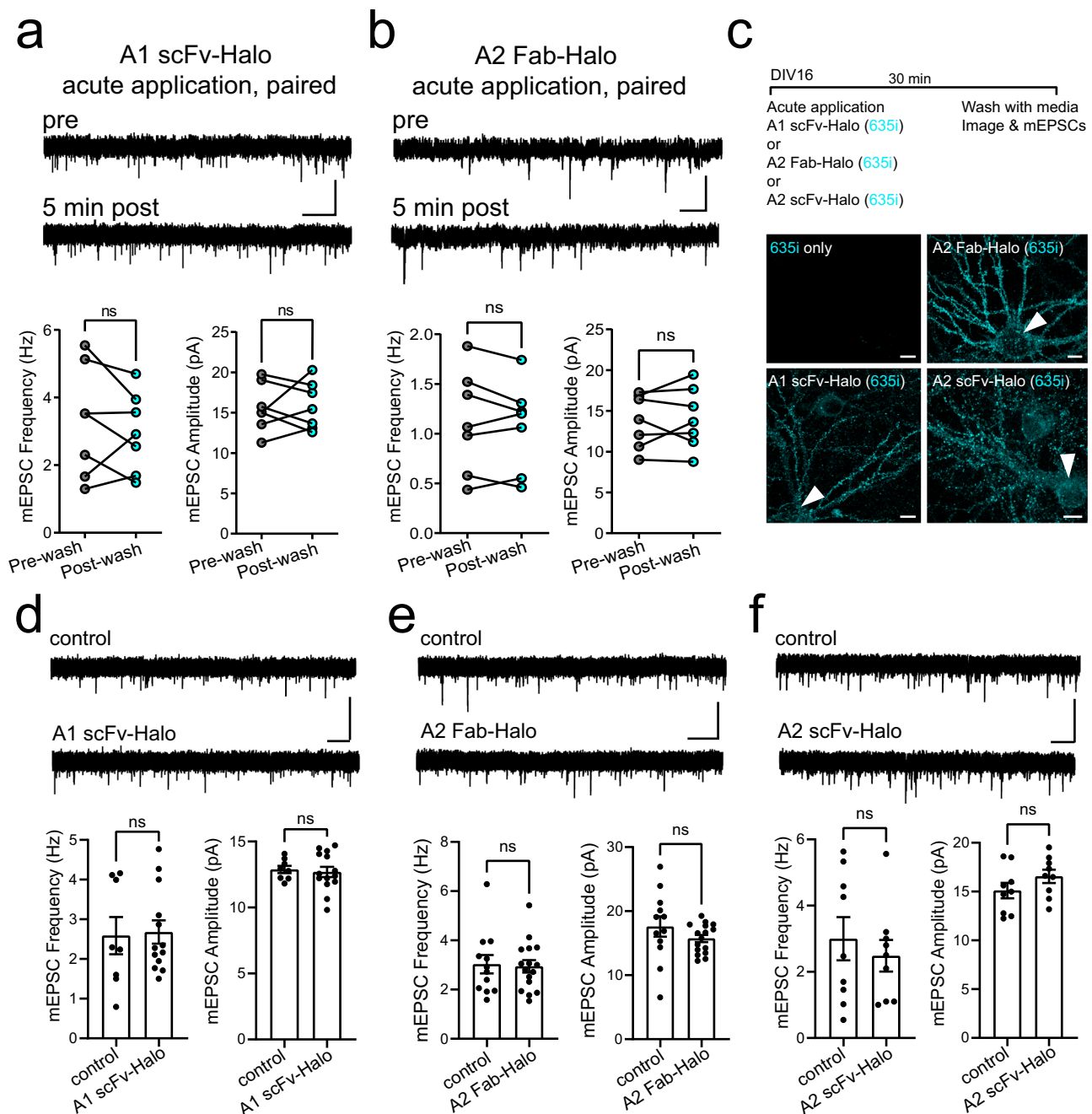


**Fig. 2 | Functional characterization of R-mAb-bound AMPARs.** **a** Representative mEPSCs traces from a dissociated hippocampal neuron before (pre) and after (5 min post) acute application of A1 scFv-Halo (scale bar is 15 pA/1 s). mEPSC frequencies and amplitudes, paired from the same cells pre- and post-A1 scFv-Halo application are shown below ( $n = 7$  cells from 2 cultures, two-tailed Paired t-tests: frequency n.s.  $p = 0.4247$ , amplitude n.s.  $p = 0.8433$ ). **b** Same as (**a**) but with application of A2 Fab-Halo (scale bar is 15 pA/1 s) ( $n = 7$  cells from 2 cultures, two-tailed Paired t-tests: frequency n.s.  $p = 0.4523$ , amplitude n.s.  $p = 0.6656$ ). **c** Experiment timeline (top) and representative images of cultured hippocampal neurons (bottom) treated with A1 or A2 R-mAbs pre-conjugated with JF635i or JF635i dye only (control) for 30 min. White arrowheads denote the targeted cell. Scale bars are

10  $\mu\text{m}$ . **d** Representative mEPSCs traces from control neurons and neurons labeled with A1 scFv-Halo (scale bar is 15 pA/1 s). mEPSC frequency and amplitude are shown below (control  $n = 8$  neurons, A1 scFv-Halo  $n = 13$  neurons from 2 experiments, two-tailed Student's t-tests: frequency n.s.  $p = 0.8651$ , amplitude n.s.  $p = 0.7421$ ). **e** Same as (**d**) but with A2 Fab-Halo (JF635i) (scale bar is 15 pA/1 s) (control  $n = 12$  neurons, A2 Fab-Halo  $n = 16$  neurons, two-tailed Student's t-tests: frequency n.s.  $p = 0.8503$ , amplitude n.s.  $p = 0.3848$ ). **f** Same as (**d**) but with A2 scFv-Halo (JF635i) (control  $n = 9$  neurons, A2 scFv-Halo  $n = 9$  neurons, two-tailed Student's t-tests: frequency n.s.  $p = 0.5337$ , amplitude n.s.  $p = 0.1371$ ). Data are presented as mean values  $\pm$  SEM. n.s. not significant. Source data are provided as a Source Data file.

glutamate receptors (NMDARs), which leads to elevated synaptic AMPAR responses<sup>34–36</sup>. In dissociated hippocampal neurons genetically expressing A1 scFv-Halo, we observed robust homeostatic scaling, measured as increased mEPSC amplitude, that was indistinguishable from controls (Fig. 5a,b). We also tested if A1 scFv-Halo interferes with

LTP. Here we injected AAVs encoding A1 scFv-Halo or GFP (control) into hippocampal region CA1 of post-natal day 14 (P14) mice and waited 2–3 weeks before measuring LTP in acute hippocampal slices (Fig. 5c). Live slices were incubated with cell-permeant JF585 to identify A1 scFv-Halo expressing cell bodies in CA1 for targeted patch-clamp

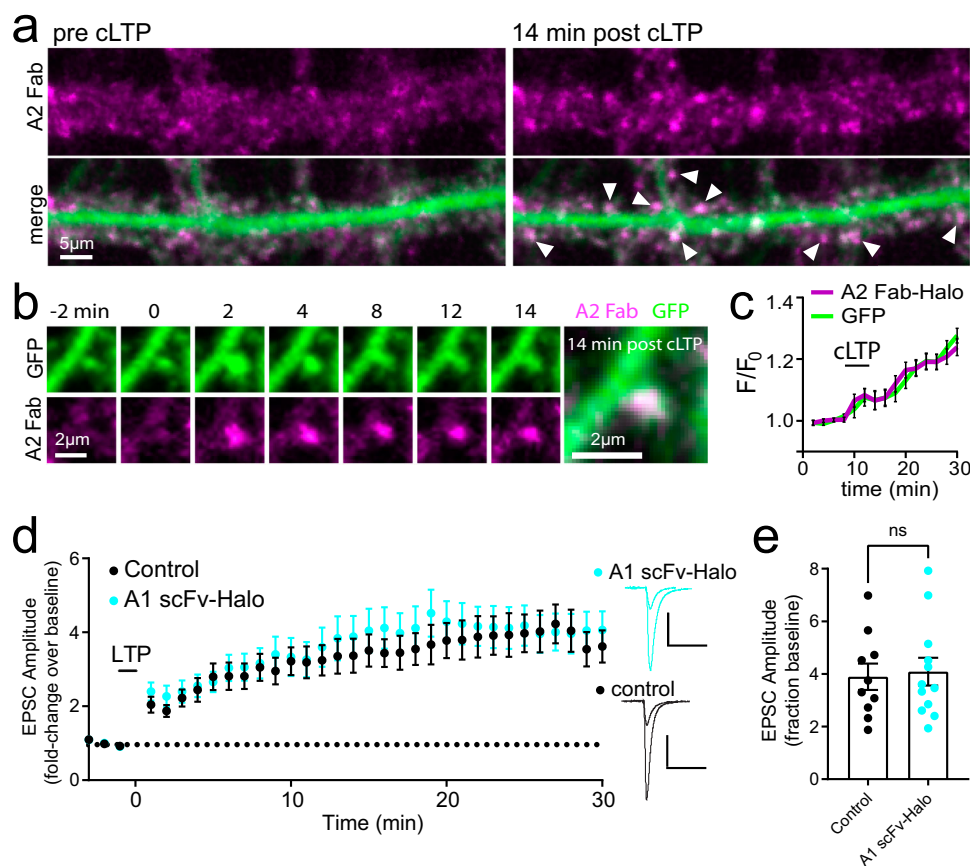


**Fig. 3 | R-mAbs do not interfere with plasticity-induced AMPAR synaptic recruitment.** **a** Representative images of a live-cultured hippocampal neuronal dendrite expressing an AAV encoding GFP and labeled with A2 Fab-Halo directly conjugated to JF549i before (left) and 14 min post cLTP treatment (right). White arrows indicate spine accumulation of A2 Fab-Halo in response to the cLTP treatment. **b** Representative images of an individual dendritic spine from a live, cultured hippocampal neuron expressing GFP-AAV and labeled with A2 Fab-Halo directly conjugated to JF549i from baseline (-2 min) to 14 min post cLTP treatment. **c** A2 Fab-Halo signal (magenta) was quantified at spines undergoing structural plasticity as measured by increased GFP cell fill intensity (green) ( $n = 75$  spines from 5 cells). **d** Plot of EPSC amplitudes (normalized to baseline responses) from CA1 pyramidal

neurons before and after LTP induction (timing denoted on plot) comparing control (JF635i only) or A1 scFv-Halo/JF635i treated groups (control  $n = 10$  neurons from 10 acute slices from 5 mice, A1 scFv-Halo  $n = 12$  neurons from 12 acute slices from 4 mice). Representative EPSC traces (right) are shown from baseline and 30-min post-LTP. Scale bars are 100 pA/200 ms. **e** Plot comparing EPSC amplitudes (normalized to baseline) 30 min following LTP induction for control (JF635i only) and A1 scFv/JF635i-treated slices (control  $n = 10$  neurons from 10 acute slices from 5 mice, A1 scFv-Halo  $n = 12$  neurons from 12 acute slices from 4 mice, two-tailed Student's  $t$ -test, n.s.  $p = 0.7955$ ). Data are presented as mean values  $\pm$  SEM. n.s. not significant. Source data are provided as a Source Data file.

recordings (Fig. 5d). LTP was triggered by pairing 0 mV depolarization with 2 Hz stimulation for 90 sec. This protocol triggered robust LTP that was nearly identical in magnitude and kinetics in cells infected with GFP-AAV or A1 scFv-Halo AAV (Fig. 5e,f). Together these data show that genetically expressed A1 scFv-Halo does not interfere with basal synaptic transmission or plasticity mechanisms that rely on regulated AMPAR trafficking to the postsynaptic membrane.

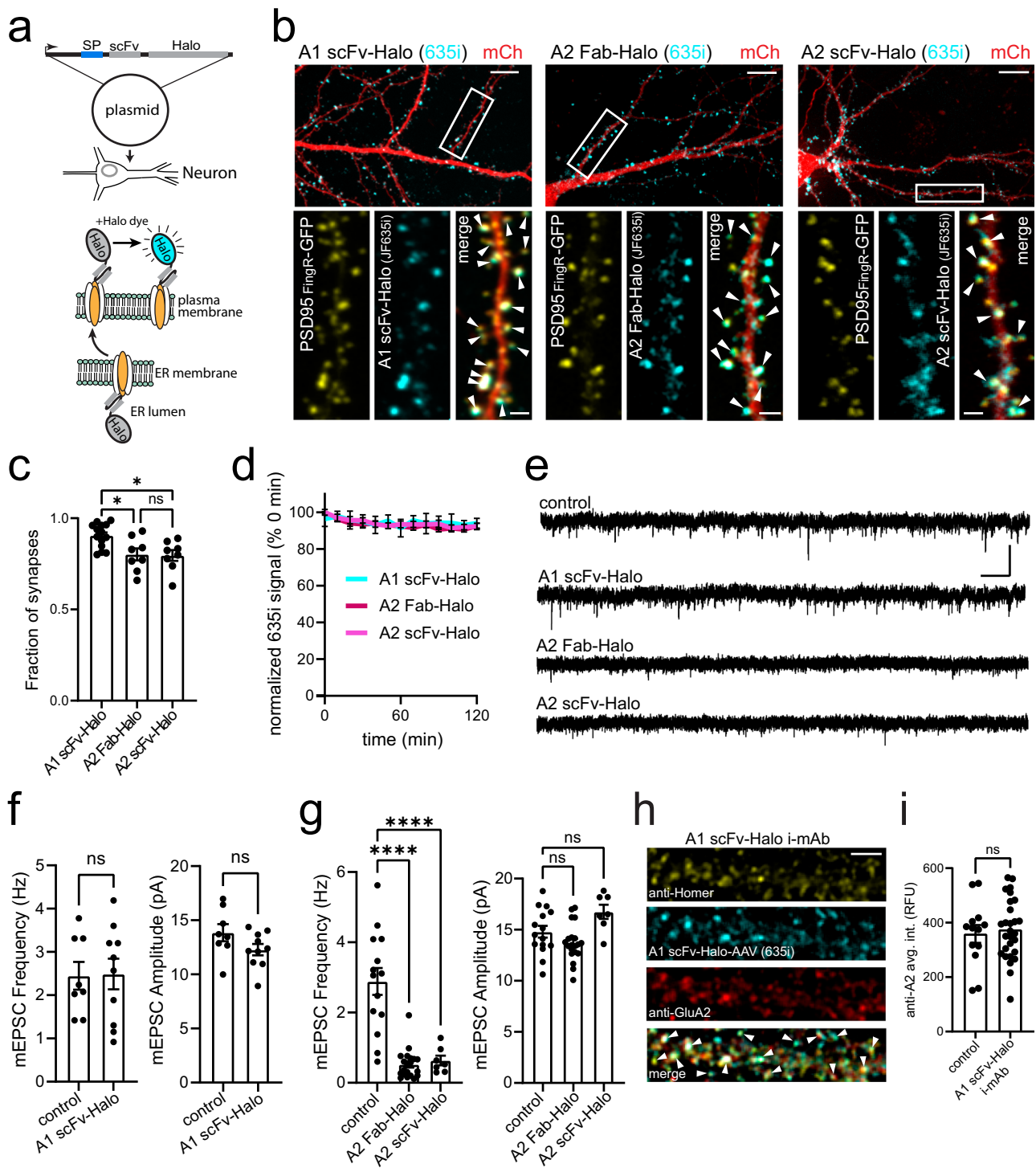
### R-mAbs and i-mAbs label synaptic AMPARs

A potential issue with labeling synaptic receptors is the access of the probe to receptors residing within the synaptic cleft<sup>37</sup>. To further characterize whether our probes can access receptors localized to the PSD, we used stimulated emission depletion (STED) microscopy to compare the nanoscale distribution of R-mAb/i-mAb-labeled receptors to conventional surface labeling with IgG antibodies. As a simple measure of synaptic localization, we quantified the fraction of the total spine AMPAR signal that overlapped with PSD95 label in our STED images. For A1 and A2 R-mAbs, we observed no significant differences compared to IgG-based commercial (GluA2) or custom-made (GluA1) antibodies (Fig. 6a-f). In all cases, we observed a wide range of AMPAR/PSD95 overlap, with some synapses displaying little overlap and others

nearly complete overlap, consistent with our previous study using higher resolution single molecule localization microscopy<sup>38</sup>. We also observed consistently lower AMPAR/PSD95 overlap when comparing GluA2 to GluA1 (regardless of labeling probe), which may reflect a small population of synaptic AMPARs refractory to GluA2 labeling with any of the reagents (e.g. the epitope is masked) and/or a larger fraction of extrasynaptic GluA2-containing (e.g. GluA2/3) AMPARs. We also characterized synaptic AMPAR labeling with genetically expressed (i-mAb) A1 scFv-Halo (we did not further characterize A2 i-mAbs given their impairment of basal transmission). A1 scFv i-mAb-labeled AMPARs exhibited a nearly identical degree of PSD95 overlap compared to conventional surface labeling with a GluA1 IgG antibody or exogenously added A1-scFv R-mAb (Fig. 6a-c). Together these data confirm that our labeling reagents can infiltrate the synaptic cleft to bind synaptic AMPARs when either genetically expressed (i-mAbs) or added exogenously (R-mAb).

### Using ER-retained i-mAbs to manipulate surface AMPAR levels

Previous approaches have been developed for manipulating the surface expression of overexpressed proteins, including AMPARs<sup>39–42</sup> by retaining them in the ER. However, these approaches generally rely on



overexpressed receptor subunits and nonphysiological subunit assemblies. To manipulate the surface expression of *endogenous* AMPAR subunits, we appended the four amino acid Lys-Asp-Glu-Leu (KDEL) ER-retrieval signal<sup>41,43–45</sup> to the C-terminus of A1 scFv-Halo and A2 scFv-Halo (Fig. 7a). To test the efficacy of this strategy, we transfected cultured hippocampal neurons with A1 scFv-Halo-KDEL or A2 scFv-Halo-KDEL along with GFP-GluA1 or GFP-GluA2, respectively. GFP-tagged AMPARs at the cell surface were quantified 1–2 days post-transfection by adding Alexa647-conjugated anti-GFP to the extracellular solution. Co-expression of the KDEL scFvs severely impaired surface trafficking of overexpressed GFP-tagged AMPAR subunits relative to the same scFvs lacking the KDEL motif (Fig. S5a,b).

We next tested whether A1 or A2 scFv-KDELs block the forward trafficking of endogenous AMPARs. We first measured the subcellular localization of AMPARs in neurons expressing A1 or A2 scFv-KDEL for 3 days by immunostaining with an antibody against the intracellular GluA1 C-terminus (to avoid competition with the A1 scFv-KDEL, which binds to the extracellular N-terminus) in fixed and permeabilized neurons. While GluA1 staining strongly colocalized with the PSD marker Homer1 in control neurons (expressing an ER-retained nanobody directed against a GFP epitope), in A1 or A2 scFv-KDEL expressing neurons it appeared strongly ER localized with little synaptic localization (Fig. S5c–e). To confirm scFv-KDEL reagents do not have a general impact on all ER-processed receptors, we measured NMDAR

**Fig. 4 | R-mAbs can be genetically expressed in neurons as intrabodies.**

**a** Schematic of i-mAb approach. **b** Representative images of live hippocampal neurons transfected with designated i-mAb (cyan) along with mCherry cell fill (red) and PSD95<sup>FingR</sup>-GFP (yellow). Arrowheads indicate colocalization of i-mAbs with PSD95<sup>FingR</sup>-GFP. Scale bars are 10  $\mu$ m, insets are 5  $\mu$ m. **c** Fraction of PSD95<sup>FingR</sup>-GFP puncta, averaged per cell, with detectable GluA1 or GluA2 i-mAb signal (A1 scFv-Halo  $n = 14$  neurons, A2 Fab-Halo  $n = 8$  neurons, A2 scFv-Halo  $n = 8$  neurons, Tukey's multiple comparisons test, A1 scFv-Halo vs. A2 Fab-Halo  $*p = 0.0164$ , A1 scFv-Halo vs. A2 scFv-Halo  $*p = 0.0110$ , A2 Fab-Halo vs. A2 scFv-Halo n.s.  $p = 0.9883$ ). **d** Quantification of designated i-mAb signal stability, normalized to signal immediately following JF635i washout at  $t = 0$  (A1 scFv-Halo  $n = 35$  dendrite ROIs, A2 Fab-Halo  $n = 20$  dendrite ROIs, A2 scFv-Halo  $n = 40$  dendrite ROIs all from 2 cultures). **e** Representative mEPSC traces from neurons transfected with plasmids encoding control (antibody heavy-chain only) or designated i-mAb (scale bar is 15 pA/1 s). **f** mEPSC frequency (left) and amplitude (right) from neurons transfected with A1

scFv-Halo compared to control (control  $n = 8$  neurons, A1 scFv-Halo  $n = 10$  neurons, two-tailed Student's  $t$ -tests: frequency n.s.  $p = 0.9369$ ; amplitude n.s.  $p = 0.1044$ ). **g** mEPSC frequency (left) and amplitude (right) from neurons transfected with control, A2 Fab-Halo, or A2 scFv-Halo i-mAbs (control  $n = 14$  neurons, A2 Fab-Halo  $n = 20$  neurons, A2 scFv-Halo  $n = 7$  neurons, Dunnett's multiple comparisons test: frequency control vs. A2 Fab-Halo  $****p < 0.0001$ , control vs. A2 scFv-Halo  $****p < 0.0001$ ; amplitude control vs. A2 Fab-Halo n.s.  $p = 0.2139$ , control vs. A2 scFv-Halo n.s.  $p = 0.0695$ ). **h** Image of a hippocampal neuron dendrite that was infected with A1 scFv-Halo AAV and labeled with JF635i (cyan), anti-Homer (yellow), and anti-GluA2 (red). Arrowheads indicate A1 scFv-Halo colocalization with anti-Homer and anti-GluA2. Scale bar is 5  $\mu$ m. **i** Plot of synaptic anti-GluA2 intensity in control neurons compared to neurons expressing A1 scFv-Halo AAV (control  $n = 13$  cells, A1 scFv-Halo AAV  $n = 28$  cells, two-tailed Student's  $t$ -test, n.s.  $p = 0.6835$ ). Data are presented as mean values  $\pm$  SEM. n.s. not significant. Source data are provided as a Source Data file.

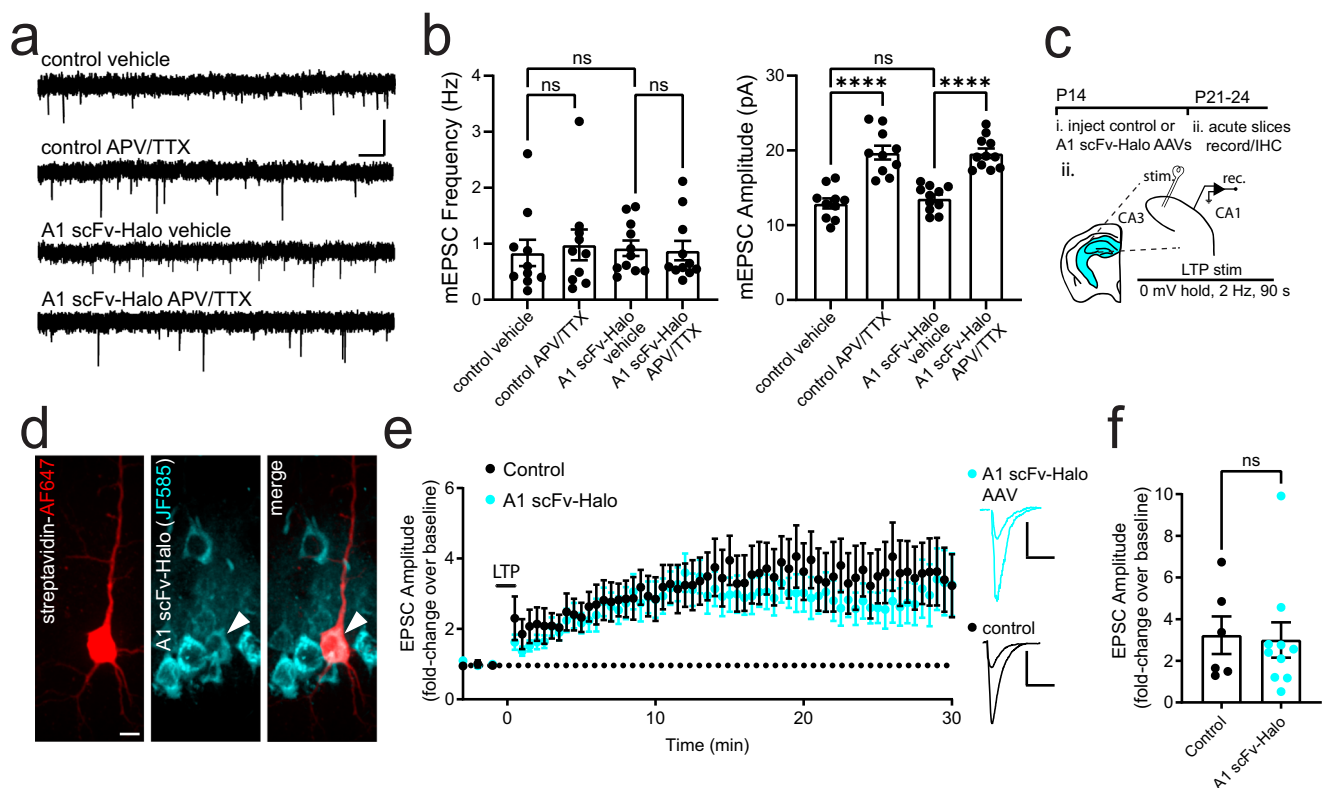


**Fig. 5 | Functional characterization of i-mAb AMPAR labeling reagents.** **a** mEPSC traces from neurons expressing A1 scFv-Halo and controls, incubated with either vehicle or 2  $\mu$ M tetrodotoxin/100  $\mu$ M APV for 24 hr to induce homeostatic scaling (scale bar is 15 pA/1 s). **b** mEPSC frequency (left) and amplitude (right) from control neurons or neurons expressing A1 scFv-Halo 24 h following vehicle or APV/TTX treatment (control vehicle  $n = 10$  neurons, control APV/TTX  $n = 10$  neurons, A1 scFv-Halo vehicle  $n = 11$  neurons, A1 scFv-Halo APV/TTX  $n = 11$  neurons all from 2 cultures, Tukey's multiple comparisons test, frequency control vehicle vs. control APV/TTX n.s.  $p = 0.9632$ , A1 scFv-Halo vehicle vs. A1 scFv-Halo APV/TTX n.s.  $p = 0.9988$ , control vehicle vs. A1 scFv-Halo vehicle n.s.  $p = 0.9916$ ; amplitude control vehicle vs. control APV/TTX  $****p < 0.0001$ , A1 scFv-Halo vehicle vs. A1 scFv-Halo APV/TTX  $****p < 0.0001$ , control vehicle vs. A1 scFv-Halo vehicle n.s.  $p = 0.9045$ ). **c** Hippocampal slices from mice expressing either A1 scFv-Halo-AAV or

GFP-AAV (control) for 2 weeks were prepared for electrophysiological LTP recordings and IHC. **d** Example image of a CA1 principal neuron filled with biocytin from the recording pipette (stained with streptavidin, red) to confirm A1 scFv-Halo expression (JF585, cyan) (scale bar is 10  $\mu$ m). **e** Plot of EPSC amplitudes (normalized to baseline) comparing LTP in CA1 pyramidal neurons expressing A1 scFv-Halo compared to control (infected with GFP-AAV) (control  $n = 6$  neurons from 6 slices, A1 scFv-Halo  $n = 10$  neurons from 10 slices). Representative EPSC traces pre- and 30 min post-LTP induction are shown to the right. Scale bars are 100 pA/200 ms. **f** Plot of normalized EPSC amplitudes 30 min post-LTP stimulus comparing control and A1 scFv-Halo expressing neurons (control  $n = 6$  neurons from 6 slices, A1 scFv-Halo  $n = 10$  neurons from 10 slices, two-tailed Student's  $t$ -test, n.s.  $p = 0.8626$ ). Data are presented as mean values  $\pm$  SEM. n.s. not significant. Source data are provided as a Source Data file.

function by monitoring the number and size of NMDAR-dependent quantal calcium transients (QCTs) with the calcium sensor GCaMP6s as previously described<sup>46</sup> (Fig. S6a-c). We observed no change in QCT frequency, and a modest but significant increase in QCT amplitude when the A1 scFv-Halo-KDEL was expressed, indicating NMDAR function is intact, even when AMPAR transmission is severely impaired

(Fig. S6c). Whether the lack of AMPAR signaling leads to increased NMDAR  $\text{Ca}^{2+}$  entry through changes in NMDAR subunit composition, abundance or synaptic localization remains to be seen. As an independent test of AMPAR scFv-KDEL specificity, we also recorded GABA<sub>A</sub> receptor-mediated miniature inhibitory postsynaptic currents (mIPSCs) from neurons expressing A1 scFv-Halo-KDEL. mIPSC

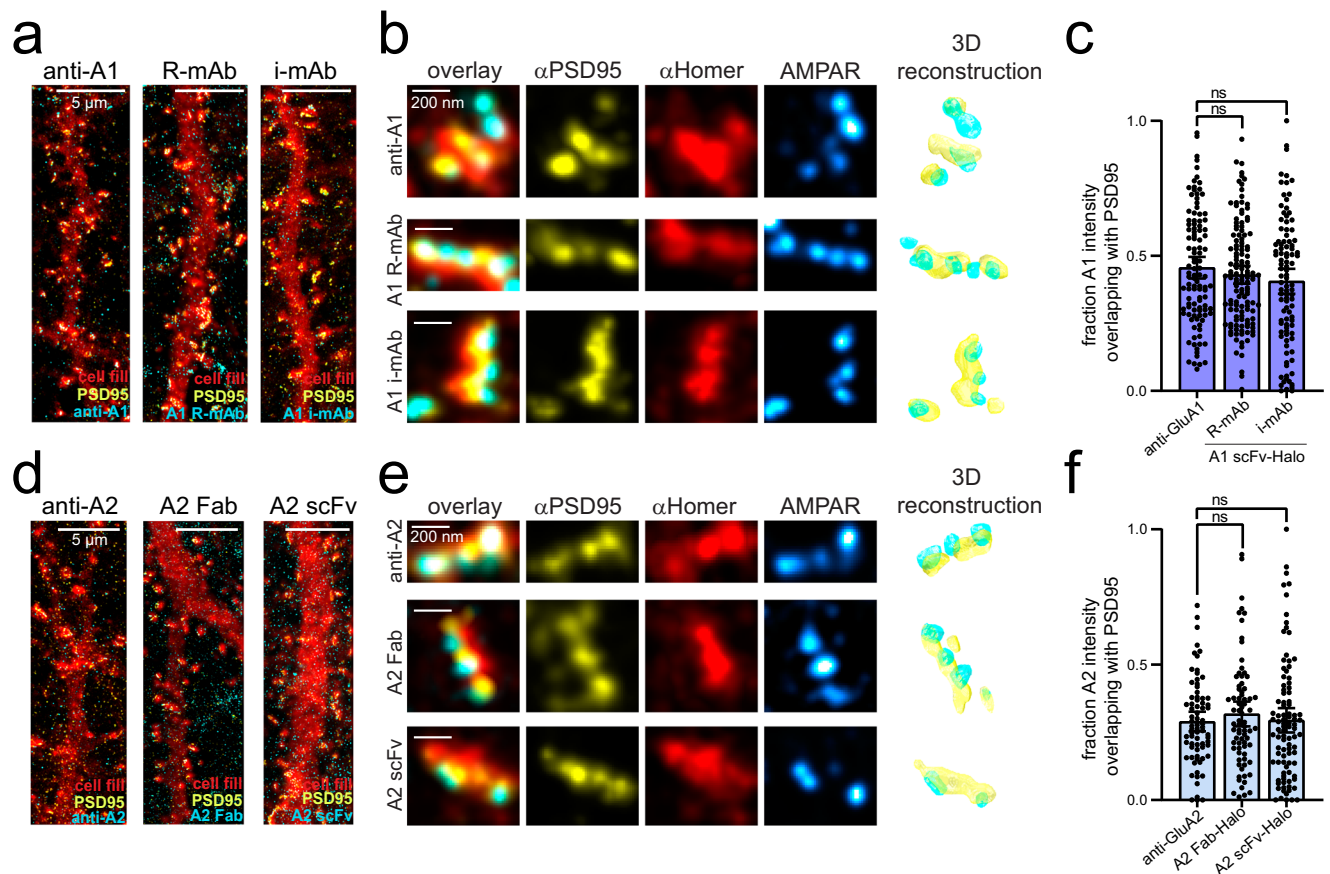


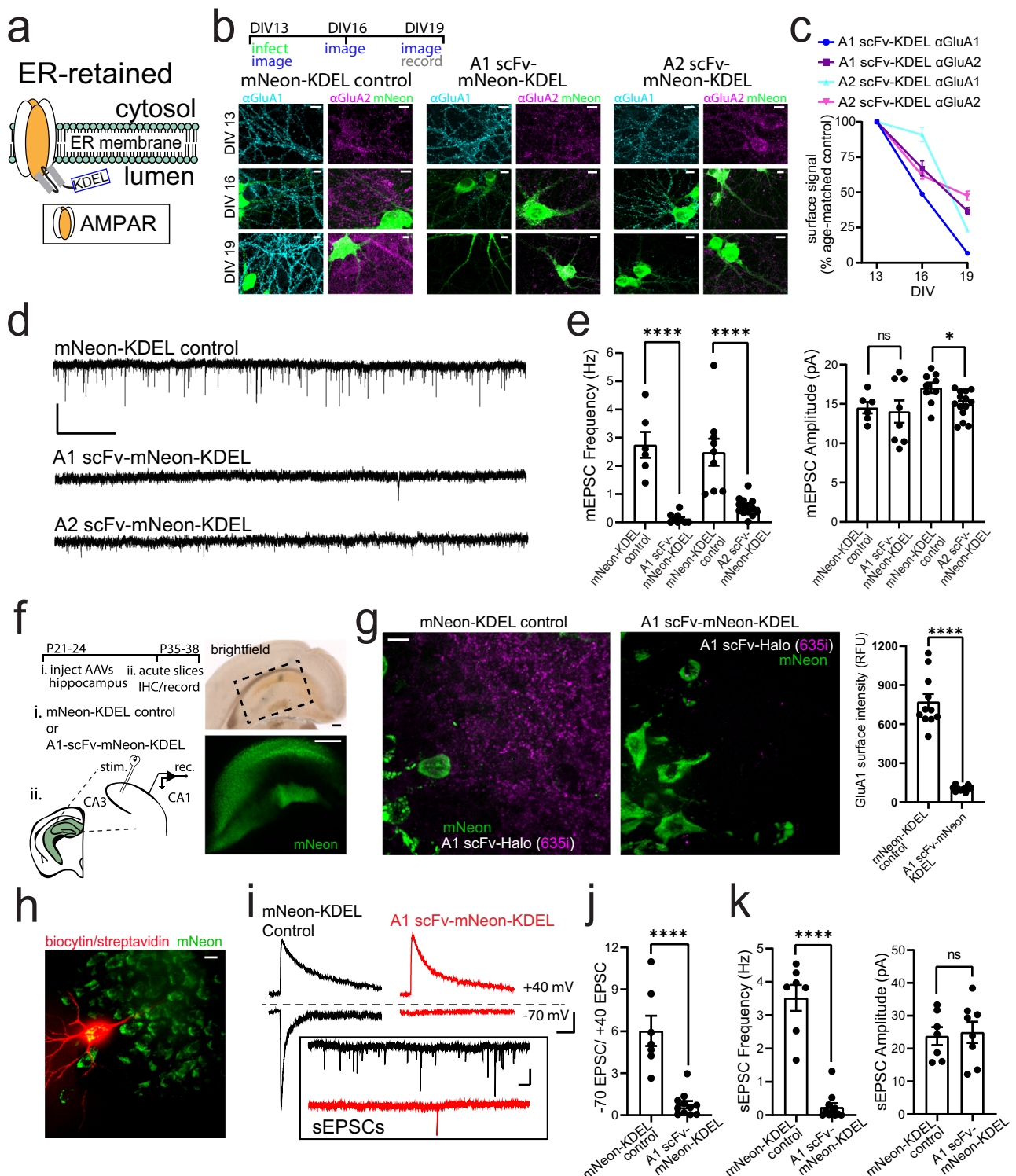
**Fig. 6 | Validation of R-mAbs and i-mAbs for labeling synaptic AMPARs.** **a** STED images show primary hippocampal dendrites from GFP-expressing neurons (red) labeled with A1 IgG antibody (left), A1 scFv R-mAb (middle) or A1 scFv i-mAb (right) (cyan) along with immunostaining for PSD95 (yellow). **b** Higher magnification images show individual dendritic spines labeled with anti-PSD95 (yellow), anti-Homer1 (red) or conventional anti-GluA1, A1 scFv-Halo R-mAb, or A1 scFv-Halo i-mAb (blue) and 3D reconstructions of the same synapses. **c** Fraction of A1 intensity inside PSD95 nanodomain is plotted (anti-A1  $n = 147$  synapses from 6 cells from 2 cultures, A1 R-mAb  $n = 163$  from 5 cells from 1 culture, A1 i-mAb  $n = 121$  from 6 cells from 2 cultures, Dunnett's multiple comparisons test, anti-A1 vs. A1 R-mAb n.s.  $p = 0.7873$ , anti-A1 vs. A1 i-mAb n.s.  $p = 0.0539$ ). **d** STED images of primary

hippocampal dendrites expressing GFP (red) and labeled with anti-PSD95 (yellow) and either A2 IgG antibody (left), A2 Fab-Halo R-mAb (middle) or A2 scFv-Halo R-mAb (right) (cyan). **e** Higher magnification images show individual dendritic spines labeled with anti-PSD95 (yellow), anti-Homer1 (red) or conventional anti-GluA2, A2 Fab-Halo R-mAb, or A2 scFv-Halo R-mAb (blue) and 3D reconstructions of the same synapses. **f** Plot of fraction of A2 intensity inside PSD95 nanodomain (anti-A2  $n = 88$  synapses from 6 cells from 2 cultures, A2 Fab-Halo R-mAb  $n = 162$  from 8 cells from 2 cultures, A2 scFv-Halo R-mAb  $n = 131$  from 6 cells from 1 culture, Dunnett's multiple comparisons test, anti-A2 vs. A2 Fab-Halo R-mAb n.s.  $p = 0.3927$ , anti-A2 vs. A2 scFv-Halo R-mAb n.s.  $p = 0.3756$ ). Data are presented as mean values  $\pm$  SEM. n.s. not significant. Source data are provided as a Source Data file.

frequency and amplitude were nearly identical in A1 scFv-Halo-KDEL neurons compared to controls (Fig. S6d,e). Together, these results confirm these reagents do not have a general effect on ER protein biosynthesis, processing, or trafficking of other excitatory or inhibitory synaptic receptors.

We next tested whether our scFv-KDEL reagents could be used to manipulate AMPAR trafficking in vivo. To this end, we generated adeno-associated viral (AAV) vectors encoding A1 and A2 scFvs fused to the green fluorescent protein mNeon, an HA-tag, and the C-terminal KDEL motif (scFv-mNeon-KDEL) (Fig. 7b). We first confirmed that viral expression levels of A1 and A2 scFv-mNeon-KDEL were sufficient to block AMPAR surface expression in cultured neurons. We observed significant reductions in surface GluA1 and GluA2 following 3 days of infection with A1 or A2 scFv-mNeon-KDEL AAVs, compared to controls (Fig. 7b,c). Moreover, GluA2 surface levels were reduced when GluA1 was retained and vice versa, consistent with the assembly and retention of GluA1/2 heteromeric AMPARs in the ER (Fig. 7c). Accordingly, AMPAR-mediated mEPSC frequency was severely reduced 6 days following infection with either A1 or A2 scFv-mNeon-KDEL AAVs (Fig. 7d,e). To test if this approach could block AMPAR function in vivo, we injected AAVs encoding A1 scFv-

mNeon-KDEL or a control construct lacking the A1 scFv (mNeon-KDEL) into the hippocampus of post-natal day 21 (P21) mice (Fig. 7f). We prepared acute hippocampal slices 2-3 weeks later and measured surface GluA1 levels by incubating live slices with recombinant A1 scFv-Halo. We observed severely reduced surface GluA1 signal in the A1 scFv-mNeon-KDEL expressing slices compared to controls (Fig. 7g). To confirm reduced labeling was not due to a fraction of the A1 scFv-mNeon-KDEL escaping the ER, potentially occluding subsequent A1 scFv-Halo surface labeling, we also stained live slices with an antibody against the HA epitope included on A1 scFv-mNeon-KDEL. Under non-permeabilized conditions, we observed no detectable anti-HA signal (Fig. S7a,c). We confirmed our HA antibody can detect this construct by repeating the staining with permeabilized slices (Fig. S7b,c). Together these results demonstrate robust ER retention of GluA1. This experiment also validates the use of R-mAbs as reagents for slice immunohistochemistry (Fig. 7g, S7a). To test if AMPAR-mediated excitatory transmission was impaired in neurons expressing A1 scFv-mNeon-KDEL (Fig. 7h), we measured electrically evoked AMPAR and NMDAR currents from infected CA1 pyramidal neurons. Evoked AMPAR responses recorded at  $-70$  mV were nearly eliminated in A1 scFv-mNeon-KDEL expressing neurons



while NMDAR responses recorded at +40 mV were intact, with the AMPAR to NMDAR EPSC amplitude ratios reduced nearly 10-fold compared to controls (Fig. 7i,j). We also observed reduced spontaneous EPSC frequency (control  $3.52 \pm 0.39 \text{ s}^{-1}$ , KDEL  $0.24 \pm 0.12 \text{ s}^{-1}$ ) with no change in amplitude (control  $23.8 \pm 2.72 \text{ pA}$ , KDEL  $24.96 \pm 3.27 \text{ pA}$ ) (Fig. 7i,k), similar to our mEPSC measurements in cultured hippocampal neurons. Together these data show that i-mAbs can be used as simple, genetically encoded loss-of-function tools in vitro and in vivo. Moreover, in contrast to previous work suggesting synaptic AMPARs are primarily composed of GluA2/3-

containing AMPARs under basal conditions<sup>47</sup>, our results agree with more recent conditional knockout and structural studies supporting a major role for GluA1-containing AMPARs for basal synaptic transmission<sup>14,19</sup>.

## Discussion

Here we describe the development and validation of antibody-based affinity reagents for visualizing and manipulating endogenous AMPARs. These reagents provide a simple approach for investigating and disrupting protein localization, function, and trafficking. More

**Fig. 7 | Manipulating AMPAR surface trafficking with R-mAbs.** **a** Approach for AMPAR ER retention. **b** Experimental timeline and images of cultured hippocampal neurons infected with AAVs encoding control (mNeon-KDEL) or designated i-mAb-KDEL, labeled with surface anti-GluA1 (cyan) or anti-GluA2 (magenta) (scale bars are 10  $\mu$ m). **c** Quantification of GluA1 or GluA2 surface staining at different timepoints as a percentage of age-matched control neurons ( $n = 7$  ROIs from 2 coverslips per timepoint). **d** mEPSC traces from cultured hippocampal neurons infected with designated AAVs (scale bar is 20 pA/5 s). **e** Quantification of mEPSC frequencies (mNeon-KDEL control  $n = 6$ , A1 scFv-mNeon-KDEL  $n = 9$  neurons, two-tailed Student's t-test, \*\*\*\* $p < 0.0001$ ; mNeon-KDEL control  $n = 9$ , A2 scFv-mNeon-KDEL  $n = 14$  neurons, two-tailed Student's t-test, \*\*\*\* $p < 0.0001$ ) and amplitudes (mNeon-KDEL control  $n = 6$ , A1 scFv-mNeon-KDEL  $n = 8$ , two-tailed Student's t-test n.s.  $p = 0.7836$ ; mNeon-KDEL control  $n = 9$ , A2 scFv-mNeon-KDEL  $n = 14$  neurons, two-tailed Student's t-test, \* $p = 0.0128$ ). **f** Experimental setup and image of hippocampal slice expressing A1 scFv-mNeon-KDEL (scale bars: brightfield image 200  $\mu$ m, fluorescence image 200  $\mu$ m). **g** Control or A1 scFv-mNeon-KDEL expressing hippocampal slices were live labeled with A1 scFv-Halo/JF635i (magenta) prior to fixation and

imaging (scale bar is 10  $\mu$ m). Quantification (Relative Fluorescence Units) of A1 scFv-Halo/JF635i surface labeling is also plotted (control,  $n = 11$  ROIs from 4 slices, A1 scFv-mNeon-KDEL  $n = 11$  ROIs from 4 slices, two-tailed Student's t-test \*\*\*\* $p < 0.0001$ ). **h** Example of a recorded (biocytin-filled) CA1 neuron to confirm A1 scFv-mNeon-KDEL expression (green) (scale bar is 10  $\mu$ m). **i** Electrically-evoked currents were recorded at +40 mV (AMPA + NMDARs) or -70 mV (AMPARs) from mNeon-KDEL control (black) or A1 scFv-mNeon-KDEL (red) neurons (scale bar is 100 pA/20 ms). Inset shows sEPSCs (scale bar is 20 pA/0.5 s). **j** AMPAR:NMDAR current ratios from mNeon-KDEL control or A1 scFv-mNeon-KDEL neurons (control  $n = 7$  cells, A1 scFv-mNeon-KDEL  $n = 11$  cells, two-tailed Student's t-test, \*\*\*\* $p < 0.0001$ ). **k** sEPSC frequencies and amplitudes from mNeon-KDEL control or A1 scFv-mNeon-KDEL neurons (frequency: control  $n = 7$  cells, A1 scFv-mNeon-KDEL  $n = 11$  cells, two-tailed Student's t-test, \*\*\*\* $p < 0.0001$ ) (amplitude: control  $n = 7$  cells, A1 scFv-mNeon-KDEL  $n = 8$  cells, two-tailed Student's t-test, n.s.  $p = 0.7911$ ). Data are presented as mean values  $\pm$  SEM. n.s. not significant. Source data are provided as a Source Data file.

broadly, this work provides a template for developing similar reagents against diverse protein targets as more monoclonal antibody sequences become available.

With any new toolset, there are advantages and limitations. The most significant advantage is the ability to label, track and manipulate endogenous proteins in live cells without overexpressing tagged proteins. While recent advances in CRISPR-mediated gene editing have addressed the limitations of overexpression, these approaches generally require introduction of multiple components (cas9, gRNA, knock-in cassette) making them inefficient in differentiated cells like neurons and difficult to multiplex with additional genetically encoded tools or probes<sup>1,2,4,5</sup>. Furthermore, CRISPR-based knock-in approaches can lead to the disruption of one or both alleles through insertion/deletion mutations. This is especially problematic when labeling proteins at or near their N-termini, although in some cases targeting intronic sequences can overcome this issue<sup>3,5</sup>. Finally, fusing fluorescent probes to target proteins can disrupt localization and/or function. For example, expressed N-terminally tagged GFP-GluA1 can be excluded from synapses under basal conditions, especially in intact circuitry<sup>48</sup>, whereas R-mAb/i-mAb labeled GluA1 appears to localize and function normally. The exclusion of GFP-GluA1 from synapses does not appear due to simple steric hindrance preventing access to the synaptic cleft since the even larger R-mAb-Halo-bound AMPARs appear to functionally incorporate into the PSD under basal conditions and following plasticity. Interestingly, GluA1 lacking its N-terminal domain altogether is also poorly incorporated into synapses<sup>49</sup> suggesting a requirement for specific extracellular protein interactions within this region. Such interactions do not appear to be perturbed by the A1 R-mAb given the lack of AMPAR functional deficits or mislocalization. Our results also highlight an important limitation of our approach. While exogenously added A2 R-mAbs did not disrupt AMPAR function, the same reagents strongly impaired AMPAR-mediated transmission when genetically expressed as i-mAbs. Whether this is due to a functional deficit in subunit assembly in the ER and/or interference with early biosynthetic modifications (e.g. glycosylation) required for function or synaptic localization remains to be seen.

Our approach offers several advantages for protein loss of function, compared to genetic knockout strategies. Using our ER trapping strategy, AMPAR surface levels and function were significantly impaired within 2–4 days of induction vs ~6–12 days for cre recombinase<sup>19</sup> or CRISPR-mediated<sup>50,51</sup> genetic knockout. Since ER trapping is initiated rapidly following induction, our approach is only limited by the expression of the i-mAb and internalization/degradation kinetics of existing surface protein. AMPAR protein lifetimes have been estimated at ~3 days<sup>52</sup>, similar to the time course for decreased AMPAR surface levels and functional impairments we observe following the introduction of ER-trapping i-mAbs. ScFv open reading frames are

small enough that multiple scFvs could be packaged into a single AAV for dual or even triple loss of function experiments using a single viral vector, a major advantage compared to costly and time-consuming genetic breeding strategies. Another advantage over genetic knockout is that our approach is, in principle, reversible and tunable. For example, by combining our ER retention i-mAbs with inducible genetic expression systems (e.g., Dox on/off) or recently described opto/chemogenetic approaches<sup>41,53</sup>, one could bidirectionally manipulate receptor surface levels with spatial and temporal control. Finally, our approach offers a clear advantage when investigating the functional contributions of individual subunits of large complexes, such as AMPARs. In many cases, when single subunits are genetically deleted, non-physiological complexes can form, complicating interpretation of knockout phenotypes. For example, in GluA2 knockout animals, the remaining AMPAR subunits assemble and traffic to synapses, leading to non-physiological synaptic responses and an underestimate of the role of GluA2 in AMPAR-mediated transmission<sup>19</sup>. However, our ER-trapping approach sequesters the targeted subunit, as well as any partnering subunits in the complex. This likely explains why we observed a larger functional effect of trapping GluA2-containing AMPARs (~85% decrease in mEPSC frequency) compared to previous studies using conditional genetic deletion of the GluA2 subunit (~40% decrease in mEPSC frequency)<sup>19</sup>. Whether residual responses we observe following GluA2 ER retention are due to native homo- or heteromeric assemblies of GluA1,3,4 subunits, or incomplete retention of GluA2-containing receptors remains to be seen.

Through developing and validating our AMPAR loss-of-function approach, we also made some interesting observations concerning the relationship between AMPAR surface levels and excitatory synaptic transmission. Notably, we found that even though AMPAR surface levels were reduced several-fold, along with mEPSC frequency, the average amplitude of the remaining mEPSCs was not significantly impacted. This is similar to previous work investigating AMPAR transmission when the AMPAR scaffolding proteins PSD95, PSD93 and SAP102 were simultaneously knocked down<sup>54</sup>. Here quantal amplitude was preserved even though quantal content was severely reduced. In both cases, a sparse subset of synapses appears to maintain sufficient AMPAR content for normal responses. In our experiments, it remains to be seen if this is due to a subset of resilient synapses where AMPAR turnover is exceptionally slow, possess unique AMPARs comprised entirely of non-ER-trapped subunits, or whether a consolidation mechanism takes place to concentrate residual surface AMPARs at select synapses in the face of ebbing excitatory postsynaptic function.

While similar nanobody or intrabody-based labeling reagents have been developed for cytosolic proteins, we initially focused on antibodies against extracellular epitopes on integral membrane

proteins, due to the ease with which we could manipulate their forward trafficking by ER trapping. This also alleviated the requirement for careful control of i-mAb expression levels for protein visualization since we could use cell impermeant halo dyes to selectively label i-mAb-bound surface receptors. Indeed, with our current delivery methods, i-mAbs are almost certainly expressed in large stoichiometric excess over native AMPARs. Thus, until a suitably approach is developed to precisely match i-mAb and AMPAR expression levels, our probes would not be useful for visualizing internal, forward trafficking receptor pools since they would be obscured by free (non-AMPA bound) i-mAb signal. Finally, targeting surface epitopes also allowed us to genetically express i-mAbs within their native organelle, the ER, where they can undergo requisite post-translational modifications such as glycosylation and disulfide bond formation. Strategies have been adapted for expressing cytosolic antibody-based probes by grafting specific antibody complementarity determining regions (i.e. antigen binding motifs) onto a cytosolic-permissive scFv scaffold<sup>55</sup>, however this approach requires additional engineering and validation as well as a transcription control mechanism to ensure the probe does not over-titrate the target protein, obscuring its localization<sup>6</sup>. In any case, the growing number of available monoclonal antibody sequences against intra- and extracellular epitopes should allow the basic strategies we outline here to be implemented to generate similar probes for diverse protein targets. Merging antibody-based affinity reagents with the expanding repertoire of opto- and chemogenetic approaches for controlling protein interactions and localization will yield simple and powerful tools for visualizing and manipulating endogenous proteins with spatial and temporal precision.

## Methods

### Vertebrate animals

All procedures were conducted in accordance with guidelines approved by Administrative Panel on Laboratory Animal Care at University of Colorado, Anschutz School of Medicine, accredited by Association for Assessment and Accreditation of Laboratory Animal Care International (AAALAC) (00235) and approved under the animal protocol #0300. Timed pregnant Sprague Dawley rat dams (typically day 16) were obtained from Charles River Laboratories and housed under standard conditions (12-h light/dark cycle with food and water *ad libitum*) until the litter was born. Male and female C57BL/6 mice used for testing the R-mAbs and i-mAbs in acute brain slices were obtained from Jackson Laboratories.

### Cell lines

HEK293 cells were obtained from ATCC and maintained and propagated under standard conditions (10% FBS in DMEM, 37 °C, 5% CO<sub>2</sub>).

### Neuronal cell culture

Dissociated hippocampal neurons were prepared from both male and female neonatal Sprague-Dawley rat pups<sup>56</sup>. Rats aged 0–2 days were decapitated and the hippocampi were extracted using papain digestion. The cells were plated at a density of around 100,000 cells per well on 18-mm coverslips coated with poly-D-lysine (Sigma, P6407) in 12-well cell culture dishes containing MEM with 10% FBS (Cytiva, SH30071.02HI) and penicillin/streptomycin. After 24 hours, the medium was switched to Neurobasal-A medium (Invitrogen, 10888022) with added B27 (Invitrogen, 17504044) and Glutamax (Thermo Fisher, 35050061). The neurons were cultured at 37 °C in a humidified incubator with 5% CO<sub>2</sub>. Dissociated hippocampal neurons were transfected between 12 and 16 days in vitro (DIV) with lipofectamine 2000 (Thermo Fisher, 11668027) according to the manufacturer's protocol. Microscopy and electrophysiology experiments were performed within 48–72 hr of dissociated hippocampal culture transfection.

### Molecular cloning

The sequences and AMPAR binding sites for the variable domains used to generate A1 scFv-Halo (antibody 11B8), A2 Fab-Halo (antibody 15F1) and A2 scFv-Halo were obtained from published AMPAR structures<sup>14</sup>. An N-terminal Ig kappa signal peptide (METDTLLLVWLLLVPGSTGD) was included upstream of Fab and scFv sequences to direct them to the endoplasmic reticulum. A2 scFv-Halo was designed by connecting the GluA2-HC variable domain to the GluA2-LC variable domain using a 16-amino acid linker (SGGGSGGGSGGGSGGGS).

### Production of R-mAbs in heterologous cells

To produce R-mAbs for acute application experiments, HEK293T cells are plated and grown in 15 cm<sup>2</sup> dishes (minimum 3 dishes per R-mAb). The day before transfection, split HEK cells and seed  $\sim 10 \times 10^6$  cells in 25 ml of DMEM (10% FBS and P/S) in one 15 cm dish. The following day the cells should be  $\sim 50\%$  confluent and are ready to transfect (calcium phosphate transfection). For production of A2 Fab-Halo R-mAb, transfection of plasmids for both the heavy chain (20  $\mu$ g) and light chain (15  $\mu$ g) are required. For the scFv R-mAbs, transfection of 20  $\mu$ g per dish is required. A small amount (5  $\mu$ g) of a cell fill plasmid is also included in each transfection mixture to confirm transfection efficiency.

**Example of calcium phosphate transfection for production of A2 Fab-Halo R-mAb.** Dilute 20  $\mu$ g of the heavy chain plasmid, 15  $\mu$ g of the light chain plasmid, and 5  $\mu$ g of mCherry plasmid with 0.25 M CaCl<sub>2</sub> in 1250  $\mu$ l H<sub>2</sub>O. Gently add this DNA mixture dropwise to a separate tube containing 1250  $\mu$ l 2xHBSS (in mM): 50 HEPES, 1.4 Na<sub>2</sub>HPO<sub>4</sub>, 280 NaCl (pH 7.05). Add the transfection mixture dropwise to the cells, return the cells to the incubator for  $\sim 24$  hr. The next day (24 hr post transfection) check the cells for transfection efficiency using mCherry expression and replace the media with fresh DMEM (10% FBS and P/S). R-mAb is ready for collection in the media 27–96 hr post-transfection.

**R-mAb collection and concentration.** Collect the media containing secreted R-mAb. Try not to disturb/collect any HEK cells. Centrifuge the media at 500 $\times g$  for 5 min to pellet cell debris. Filter the media through a 0.45  $\mu$ m syringe filter. At this point, test the R-mAb on neurons to confirm its efficiency prior to concentration. Note that it is best to add to live cells, as fixation destroys the epitope. Since the HEK cell media can contain trace amounts of glutamate, incubate with APV or MK801 to prevent excitotoxicity. To concentrate the R-mAb into a different buffer, use Amicon ultra (Sigma, UFC903024) size exclusion centrifugation columns (30 kDa cutoff for the scFv-Halo R-mAbs or 50 kDa cutoff for the A2 Fab-Halo R-mAb). One Amicon column is required for every 30 ml of media (15 cm dish). Begin by washing the filter column with 5 ml PBS and centrifuge at 3000 $\times g$  for 10 min. Add 15 ml of media containing R-mAbs to the column and centrifuge at 3000 $\times g$  for 20 min. Repeat centrifugation until all of the media has been added to the column. Keep the flow-through for analysis to ensure R-mAb is being retained in the column. After all of the media has been added, you should have  $\sim 250$   $\mu$ l of concentrated R-mAb. Dilute the R-mAb with 12 ml 1x PBS and centrifuge 3000 $\times g$  for 20 min to re-concentrate. Repeat wash steps a total of 3 times to remove any residual cell media. Collect the concentrated R-mAb, aliquot to desired volume, and store at  $-80$  °C. A 6x Histidine tag has been added to the R-mAbs for further purification, if necessary, but experiments here were carried out with concentrated preps as described above.

### Direct conjugation of R-mAbs to HaloDyes

250  $\mu$ l of concentrated R-mAb, prepared as described above, were incubated with 10  $\mu$ M HaloDye for 3 hr on ice, and then 30 min at room temperature, vortexing every 30 min. R-mAb/HaloDye mixture was then desalted to remove excess HaloDye through PD SpinTrap G-25

(Cytiva, 28918004). Directly conjugated R-mAbs were then stored at 4 °C.

### CRISPR-mediated knockout of GluA1 and GluA2 for R-mAb validation

Guide RNAs targeting GluA1 and GluA2 were identified using CRISPOR<sup>57</sup> and screened for efficient knockout using a commercial antibody against GluA2 (Millipore, MAB397) or a custom antibody against GluA1<sup>38</sup>. gRNA sequences were cloned into Addgene plasmid #124844<sup>57</sup> modified for constitutive (i.e. not cre-dependent) expression of *Staphylococcus aureus* Cas9 from the human synapsin promoter. CRISPR plasmids were transfected into dissociated hippocampal neurons (along with a GFP cell fill plasmid to identify transfected cells) at DIV6-7 and processed for GluA1 or 2 antibody or R-mAb labeling 9-10 days later (DIV16-17). Briefly, cells were incubated live for 10-25 min with either antibodies or R-mAbs prior to fixation with 4% PFA in PBS (5 min at room temperature). Fixed cells were incubated with Alexa647-conjugated anti-mouse secondary antibody to label A2 Fab or JF635i to label A1 scFv-Halo. We used the following gRNA sequences (targeting rat sequences) for GluA1 and GluA2 knockout, respectively: GluA1 ACATTCTGACCAACCGAGG; GluA2 GCTACCTCCAAATTGTCGATA.

### Imaging

Live cell imaging was performed at 32°C on an Olympus IX71 equipped with a spinning disc scan head (Yokogawa). Excitation illumination was delivered from an acousto-optic tunable filter (AOTF) control laser launch (Andor). Images were acquired using a 60x Plan Apochromat 1.4 NA objective and collected on a 1024×1024 pixel Andor iXon EM-CCD camera using Metamorph (Molecular Devices) data acquisition software. For experiments performed in cultured neurons, a 4.8 μm Z-stack (0.4 μm step-size) was acquired at each time point. For experiments performed in acute and organotypic slices, a 60 μm z-stack (0.4 μm step-size) was acquired. Quantification of fluorescence intensities were performed in ImageJ. A mask of all segmented puncta was created for each image as follows: images were smoothed using the MexicanHat filter plugin (Laplacian of Gaussian) or the “Unsharp Mask” filter (Difference of Gaussians) and then thresholded manually. The average fluorescence intensity within these masked puncta was then calculated from the raw fluorescence images.

### Stability analysis of R-mAb and i-mAbs

Exogenous R-mAbs were acutely applied to live, primary hippocampal neurons for 15 min and then washed off with ~5 volumes of R-mAb-free ACSF over 1-2 min in the imaging chamber and cells imaged for up to 2 h post-wash. Expressed i-mAbs were transfected for two days. JF635i was then applied at a concentration of 1 nM for 10 min and washed out with several bath volumes of aCSF. We captured one z stack every 10 min for a total of 2 hr. The mean gray value of a 4.8 μm Z-stack was quantified from each dendritic ROI at every timepoint. Each datapoint was corrected by a bleaching factor, which was obtained by capturing the same number of images with identical laser power and exposure times using fixed cells that had been labeled identically.

### Stability analysis of A1 scFv-th-Halo i-mAb following Thrombin treatment

Primary hippocampal neurons were transfected on DIV13 with A1 scFv-th-Halo, PSD95<sub>FingR</sub>-GFP, and mCherry cell fill for three days. On DIV16, neurons were incubated with JF635i (1 nM) for 10 min and washed out with dye-free aCSF. We captured one z stack every 10 min for a total of 2 hr. At the 2 h timepoint, 2 Units of thrombin were added (Sigma, 50 units/mg, 1.12374) to the coverslip and we captured additional z stacks every 3 min for a total of 18 min. Following bleaching correction, each timepoint was normalized to the initial baseline image (time 0).

### Fluorescence Recovery After Photobleaching (FRAP)

For quantification of A1 scFv-Halo, A2 Fab-Halo and A2 scFv-Halo R-mAb mobility, primary hippocampal neuronal cultures were infected with an AAV encoding GFP to visualize cellular morphology for at least 4 days and cells were incubated with each R-mAb for 20 min followed by washout and addition of HaloDye (JF635i, 1 nM, 10 min). For quantification of i-mAb mobility, primary hippocampal neuronal cultures were infected with an AAV encoding A1 scFv-Halo for 4 days and cells were incubated with JF635i for 10 min at 1 nM. Photobleaching of individual synapses was carried out using galvanometric-steered 641 nm laser excitation (FRAPPA, Andor) at single points. No more than 5 synapses across a field of view were targeted for photobleaching. The duration and intensity of photobleaching pulses were adjusted such that they bleached no more than 60-80% of the original signal. Fluorescence recovery was monitored following photobleaching by imaging a z-stack every 60 seconds, following pre-bleach baseline acquisition.

### Analysis of R-mAb and i-mAb colocalization with conventional antibody labeling

Dissociated hippocampal neurons (DIV10) were infected with AAVs encoding GFP (for R-mAb labeling) or A1 or A2 scFv-Halo (for i-mAb labeling) for at least 4 days. Surface labeling of AMPARs using either A1 scFv-Halo R-mAb, A2 Fab-Halo R-mAb, A2 scFv-Halo R-mAb, conventional anti-GluA1<sup>25,26</sup>, conventional anti-GluA2 (Millipore MAB397), or JF635i (1 nM, for i-mAbs) was performed live for 20 min at 37 °C. Coverslips were fixed with 4% PFA in PBS (5 min at room temperature) and permeabilized with 0.2% TritonX-100 (5 min at room temperature). Cells were incubated with chicken anti-Homer1 (Synaptic Systems, 160-006) overnight at 4 °C followed by washing and secondary labeling with anti-Chicken AF568 (Thermo Fisher, A-11041) and either anti-mouse AF488 (Thermo, A28175) or anti-rabbit AF488 (Thermo Fisher, A-11008) to label anti-GluA2 or anti-GluA1, respectively, for 1 hr at room temperature. Coverslips were then mounted on Prolong Gold mounting media and cured at room temperature prior to imaging. Synaptic localization of conventional AMPAR labeling and R-mAb or i-mAb signals were quantified by generating a mask of the anti-Homer images and quantifying the presence or absence of AMPAR signal within each mask. The anti-Homer images were smoothed using Mexican Hat Filter Fiji plugin (Laplacian of Gaussian, radius=2) and Gaussian blur (sigma=1), and images were thresholded manually to generate a mask. The fraction of synapses that contained conventional anti-GluA1 or anti-GluA2 signal were then divided by the fraction of synapses that contain R-mAb or i-mAb signal or vice-versa. To quantify the colocalization of PSD95-FingR-GFP and i-mAbs, maximum projection images were manually thresholded in the PSD95-FingR-GFP channel to generate a mask (manually excluding the soma). Maximum projection images were manually thresholded in the AMPAR/i-mAb channel to determine the fraction of PSD95 puncta with i-mAb signal. Threshold values were held constant between experimental conditions.

### Analysis of R-mAb accumulation following chemical LTP

Cultured hippocampal neurons (DIV 12) were infected with an AAV encoding GFP for at least 4 days to visualize dendritic spines. Live neurons were incubated with A2 Fab-Halo directly conjugated to JF549i for 20 min at 37 °C. We utilized a cLTP induction protocol that has been previously described<sup>26</sup>. Briefly, neurons were pretreated with 2 μM TTX for 1 hr to inhibit evoked activity. Live neurons were then placed into a live imaging chamber (Ludin) and incubated in baseline aCSF containing (in mM): 130 NaCl, 5 KCl, 10 HEPES, 30 glucose, 1 MgCl<sub>2</sub>, 2 CaCl<sub>2</sub>, and 0.002 TTX (pH 7.4) and one image was acquired every 1 min for 5 min. To stimulate chemical LTP, the baseline solution was exchanged for aCSF lacking Mg<sup>2+</sup> and TTX and containing 0.2 glycine for 5 min. Following cLTP stimulation, baseline aCSF was added

lacking TTX for the remainder of the imaging period (1 image acquired every 30 sec, 30 min total).

### Analysis of R-mAb labeling in acute slices

Acute slices were incubated with A1 scFv-Halo directly conjugated to JF635i for 1–2 hr during slice recovery. Biocytin was included in the internal solution to visualize recorded cells, and slices were drop fixed in 4% PFA for 60 min, permeabilized, and stained for Streptavidin-AF488 (Thermo Fisher, S11223). We used the Streptavidin-AF488 signal to identify neurons that were recorded during these experiments (Fig. 3d,e and S2) and imaged z-stacks with 46 steps, 0.4  $\mu$ m step size, surrounding the identified dendrites. ROIs were drawn around each dendrite and the mean fluorescence intensity of the A1 scFv-Halo JF635i signal was quantified through each z-stack. The reported JF635i intensity is the signal acquired from the dendritic signal ( $\sim 4 \mu$ m in z) per dendritic ROI for each individual cell.

### Analysis of intracellular GluA1 signal comparing transfected and AAV-delivered A1 scFv-Halo i-mAbs

Cultured hippocampal neurons were transfected with A1 scFv-Halo, 200 ng/well (DIV13) for at least 2 days or infected with A1 scFv-Halo AAV (DIV11) for at least 4 days. Cells were incubated with JF635i (1 nM) for 20 min and washed 3x with aCSF prior to fixation. Coverslips were fixed with 4% PFA in PBS (5 min at room temperature) and permeabilized with 0.2% TritonX-100 (5 min at room temperature). Cells were incubated with an affinity-purified rabbit anti-GluA1 directed against the intracellular C-terminal domain<sup>31,38</sup> overnight at 4 °C followed by washing and secondary labeling with anti-Rabbit AF488 (Thermo Fisher, A-11008) for 1 hr at room temperature. Coverslips were then mounted on Prolong Gold mounting media and cured at room temperature prior to imaging. The ratio of anti-GluA1 signal in the soma vs. dendrites was quantified by drawing ROIs around the soma or dendrite regions in each cell and quantifying the mean fluorescence intensity of the anti-GluA1 signal, representing the data as a ratio of the somatic and dendritic ROI intensities.

### Quantal $\text{Ca}^{2+}$ transient analysis

Dissociated hippocampal neurons were transfected with GCamP6s<sup>59</sup> and mCherry only or mCherry plus A1 scFv-Halo-KDEL. The frequency and amplitude of spontaneous quantal  $\text{Ca}^{2+}$  transients were measured at individual dendritic spines in the green channel as previously described<sup>38</sup>. Single-plane imaging was carried out at 7 frames/sec for 1 min. Neurons were imaged in ACSF containing 1  $\mu$ M TTX, 30  $\mu$ M glycine, 2 mM  $\text{Ca}^{2+}$  but lacking  $\text{Mg}^{2+}$  to relieve NMDA receptor  $\text{Mg}^{2+}$  block. Optical quantal analysis experiments were replicated three times, using independent neuronal preparations with the number of cells and synapses analyzed.

### STED Imaging and Analysis

STED super-resolution images were acquired using the commercial Abberior STEDYCON addition to an Olympus confocal microscope equipped with the following: an Olympus UPLXAP0100XO 100X magnification and 1.45 NA. objective, 4 excitation lasers; 405(cw), 485 nm(pulsed), 561 nm(pulsed), 640 nm(pulsed), 4 corresponding single-photon counting APD detectors (avalanche photodiodes), and a 775 nm laser for stimulated emission depletion. Samples were stained using secondary antibodies labeled with Abberior STAR RED, STAR 635 and/or STAR ORANGE, STAR 580, and STAR 460 L and mounted for 24+ hours in prolong gold mounting medium. A minimum of 3 z-planes at 0.15  $\mu$ m spacing were acquired for each image and deconvolved using the SVI Huygens deconvolution software with STED object stabilization the Standard Mode Express Deconvolution, ‘conservative’ settings.

To quantify R-mAb overlap with PSD95 we used the following approach. First, regions of interest containing individual spines were

selected manually. Second, signal intensity within these regions was segmented using the ImageJ Plugin split-Bregman/MOSAIC suite<sup>60</sup>. Image segmentation was carried out on deconvolved STED images, and the following parameters were utilized: ‘Subpixel segmentation’, ‘regularization = 0.05’, ‘minimum object intensity = 0.25’, standard deviation xy = 0.8’, standard deviation = 1.1’, Local intensity estimation ‘Medium’, Noise Model ‘Poisson’. All analysis was performed blind to experimental condition. Third, a mask representing the 3D overlap of the R-mAb and PSD95 was generated using the Image J Image calculator ‘AND’ operator to combine the segmented R-mAb mask and the segmented PSD95 mask. The total intensity of the R-mAb signal within the 3D overlap mask was divided by the total R-mAb signal within the segmented 3D R-mAb mask to generate an intensity ratio that represents the fraction of R-mAb signal localized within the postsynaptic density.

### Electrophysiology in primary cultured neurons

Whole-cell patch-clamp recordings were performed using dissociated hippocampal neurons (DIV14–16) transfected with i-mAb plasmids for 2–3 days or infected with i-mAb AAVs for at least 4 days prior to recording. For acute R-mAb application experiments, a saturating dilution (previously determined by imaging) of recombinant R-mAb was added directly to the extracellular bath solution following a 5 min baseline recording period. Recordings were continued for an additional 5–10 min, which is sufficient time for R-mAbs to fully bind. Extracellular recording solution contained (in mM): 10 HEPES, 130 NaCl, 5 KCl, 30 D-glucose, 2  $\text{CaCl}_2$  and 1  $\text{MgCl}_2$  supplemented with 1  $\mu$ M tetrodotoxin (Tocris, 1069) and 30  $\mu$ M bicuculline (Tocris, 0130). Intracellular solution used for recording mEPSCs contained (in mM): 130 cesium methanesulfonate, 3  $\text{Na}_2\text{ATP}$ , 0.5  $\text{Na}_3\text{GTP}$ , 0.5 EGTA, 10 phosphocreatine, 5  $\text{MgCl}_2$ , 2.5 NaCl, 10 HEPES (290–300 mOsm). The pH was adjusted to 7.25 with CsOH. We used a high  $\text{Cl}^-$  intracellular solution for recording mIPSCs containing (in mM): 67.5 CsCl, 67.5  $\text{CsMeSO}_4$ , 0.1  $\text{CaCl}_2$ , 2  $\text{MgCl}_2$ , 10 HEPES, 0.1 EGTA, 0.5  $\text{Na}_3\text{GTP}$ , 3  $\text{Na}_2\text{ATP}$ , 10 phosphocreatine, and extracellular solution was supplemented with 1  $\mu$ M tetrodotoxin, 0.1 mM APV, and 0.01 mM NBQX. The pH was adjusted to 7.25 with CsOH. Data were collected using a multiclamp 700b amplifier and digitized using a National Instruments DAQ board and filtered at 5 KHz (single pole Bessel filter) and recorded with WinLTP software (University of Bristol). Data were analyzed using WinLTP (University of Bristol) and Mini Analysis software (Synaptosoft, version 6.0.7). Kinetic analysis of mEPSCs was achieved by fitting a 60 second segment of each trace to a variable amplitude template using pClamp 10 analysis software. Analysis was carried out blinded to the experimental condition.

### Homeostatic scaling induction in primary hippocampal neurons

Homeostatic scaling was induced by treating primary hippocampal neurons at DIV15 with 2  $\mu$ M tetrodotoxin and 0.1 mM APV for 24 hr compared with no drug control. All recordings were performed on DIV16, 24 hr post-scaling treatment with 2  $\mu$ M TTX and 0.1 mM APV were maintained in recording aCSF.

### Production of AAVs for primary culture and in vivo injection

AAV-DJ expressing R-mAb constructs were generated by co-transfecting HEK293T cells using calcium phosphate with the AAV vector (containing the R-mAb sequence) along with helper plasmids (pDJ and pHelper). Three days later, cells were harvested, lysed, and purified over an iodixanol gradient column (2 h at 63,500 rpm) in a Beckman Type80Ti rotor. The 40% iodixanol fraction containing AAV was collected, concentrated, aliquoted, and stored at  $-80^\circ\text{C}$  until use.

### Stereotactic viral injection, hippocampus

P21–24 male and female mice were anesthetized with 5% isoflurane in oxygen and kept at 1–1.5% isoflurane during surgery. Animals were head

fixed to a stereotactic frame (KOPF). An incision was made in the scalp with sterilized scissors, and small holes (~0.5 mm diameter) were drilled into the skull using a handheld dental drill. Viral solutions containing either AAV-hSYN-GluA1-scFv-mNeon-KDEL or AAV-hSYN-GFP-nb-mNeon-KDEL were injected into each hemisphere with a pulled glass micropipette. Using a syringe pump (World Precision Instruments), a total volume of 0.5  $\mu$ L was delivered into ventral hippocampus at an infusion rate of 10  $\mu$ L/hr at the following coordinates (in mm): anterior posterior: -3.10, mediolateral:  $\pm$ 3.17 (relative to Bregma), and dorsoventral: -3.45 (relative to pia). The micropipette was held in place for 5 min after injection to prevent backflow of virus, then slowly retracted. Correct localization and expression of viral infection was verified post hoc by presence of mNeon.

### Electrophysiology in acute slices

At P28-36, mice were deeply anesthetized with isoflurane and decapitated. Brains were rapidly dissected and 300  $\mu$ m horizontal slices were sectioned coronally using a vibratome (Leica VT1200) in ice cold, oxygenated solution containing (in mM) 85 NaCl, 75 sucrose, 25 D-glucose, 24 NaHCO<sub>3</sub>, 4 MgCl<sub>2</sub>, 2.5 KCl, 1.3 NaH<sub>2</sub>PO<sub>4</sub> and 0.5 CaCl<sub>2</sub>. Slices were then collected and transferred to a chamber containing oxygenated aCSF warmed to 31.5 °C containing (in mM) 126 NaCl, 26.2 NaHCO<sub>3</sub>, 11 D-Glucose, 2.5 KCl, 2.5 CaCl<sub>2</sub>, 1.3 MgSO<sub>4</sub>·7H<sub>2</sub>O, and 1 NaH<sub>2</sub>PO<sub>4</sub>, pH 7.4, followed by incubation at room temperature for at least 1 hour. During recording, slices were perfused with aCSF containing 100  $\mu$ M picrotoxin (Tocris, 1128). Hippocampal pyramidal neurons were visually identified with an Olympus BX51W microscope with a 40x dipping objective collected on a Hamamatsu ORCA-Flash 4.0 V3 digital camera using an IR bandpass filter. Cells were patched in whole-cell configuration using glass pipettes pulled to a resistance of 3-5 M $\Omega$  and filled with an internal solution containing (in mM) 130 cesium methanesulfonate, 3 Na<sub>2</sub>ATP, 0.5 Na<sub>3</sub>GTP, 0.5 EGTA, 10 phosphocreatine, 5 MgCl<sub>2</sub>, 2.5 NaCl, 10 HEPES, supplemented with Biocytin (1 mg/ml) and QX-314 bromide (10  $\mu$ M, Tocris) AMPAR- and NMDAR-mediated EPSCs were evoked by electrically stimulating CA1 axon efferents within the alveus/stratum oriens at the border of CA1 and subiculum at 0.1 Hz with a concentric bipolar electrode (FHC neural microtargeting worldwide, 30203). Cells were held at +40 mV and stimulus intensity (200  $\mu$ s pulse) was adjusted to evoke 100-400 pA NMDAR-mediated EPSCs. Evoked responses were recorded at 0.1 Hz for 2 min. Holding potential was then gradually reduced to -70 mV and AMPAR-mediated EPSCs were acquired 1 min later using the same stimulus intensity. For whole-cell LTP experiments using A1 scFv-Halo R-mAb, experimental slices were incubated for at least 2 hours in A1 scFv-Halo (JF635i) in continuously carbogen-bubbled aCSF. Synaptic responses were evoked by stimulating with a homemade nichrome electrode placed in the stratum radiatum (A-M Systems 2100 Isolated Pulse Stimulator). Following establishment of whole-cell configuration, evoked AMPAR EPSCs were recorded at -70 mV by stimulating Schaffer collateral axons at 0.1 Hz for 3-5 min. LTP was then induced by 2 Hz stimulation for 90 s with the holding potential at 0 mV. Cells were returned to -70 mV and EPSCs were measured at 0.1 Hz for up to 30 min post-LTP induction. All experiments were performed using a Multiclamp 700B amplifier and a Digidata 1550B digitizer. Recordings were collected using a 2 kHz lowpass filter and digitized at 10 kHz. All currents were analyzed using WinLTP software (version 2.32). Recordings were discarded if series resistance changed by more than 15% during the recording period.

### Immunohistochemistry in acute slices

For GluA1 or HA surface staining (probing for ER-escape of GluA1-mNeon-HA-KDEL or GFP-nb-HA-KDEL control), slices were incubated live with A1 scFv-Halo R-mAb and anti-HA (BioLegend, 901502) for 1 hr in carbogenated aCSF. Following washout with aCSF, slices were fixed with 4% PFA/PBS and then blocked with 10% BSA/ in PBS for 2 hr at

room temperature. Slices were then washed 5 times for 10 minutes each with PBS and incubated with anti-mouse AF568 for 2 hr in 5% BSA/PBS. Slices were washed again 5 times for 10 minutes each with PBS. Internal, ER-retained R-mAbs were probed by permeabilizing slices overnight with 1.5% Triton-X, blocked for 2 hr at room temperature with 10% BSA, labeled with anti-HA (BioLegend, 901502) in 5% BSA/ 0.1% Triton-X overnight at 4 °C. Slices were washed with PBS 5 times for 10 minutes and labeled with anti-mouse CF568 (Sigma, SAB4600310) in 5% BSA for 3 hr at room temperature. Slices were then washed with PBS 5 times for 10 minutes each, mounted on Vectashield antifade mounting media (Vector Laboratories), and sealed with clear nail polish.

### Quantification of total GluA1 levels when expressing KDEL i-mAbs

Dissociated hippocampal neurons (DIV10) were infected with AAVs encoding either A1 scFv-mNeon-KDEL or A2 scFv-mNeon-KDEL for 7 days. Coverslips were fixed with 4% PFA in PBS (5 min at room temperature) and permeabilized with 0.2% TritonX-100 (5 min at room temperature). Cells were incubated with chicken anti-Homer1 (Synaptic Systems, #160-006) and an affinity-purified rabbit anti-GluA1 directed against the intracellular C-terminal domain (Gift from Dr. Michael Ehlers)<sup>31,58</sup> overnight at 4 °C followed by washing and secondary labeling with anti-Chicken AF568 (Thermo Fisher, A-11041) and anti-Rabbit AF647 (Thermo Fisher, 21245) for 1 hr at room temperature. Coverslips were then mounted on Prolong Gold mounting media and cured at room temperature prior to imaging. Synaptic localization of anti-GluA1 signal was quantified by measuring the raw fluorescence intensity within a mask created using the anti-Homer images. These masks were generated by smoothing the anti-Homer images using MexicanHat Filter Fiji plugin (Laplacian of Gaussian, radius=2) and Gaussian blur (sigma=1), and then thresholding manually. Pearson's coefficients were calculated using JACoP<sup>61</sup> Fiji plugin between the mNeon-KDEL (ER) and anti-GluA1 channels.

### Antibodies used in this study

Polyclonal rabbit anti-GluA1 produced in-house (Sinnen et al., Neuron, 2017). Monoclonal anti-GluA2 (Millipore, MAB397, clone 6C4). Anti-mouse-AF647 (Thermo Fisher, 21235). Anti-rabbit-AF647 (Thermo Fisher, 21245). Anti-mouse-AF488 (Thermo Fisher, A28175). Anti-rabbit-AF488 (Thermo Fisher, A-11008). Anti-chicken-AF568 (Thermo Fisher, A-11041). Anti-PSD95-rabbit (Cell Signaling, 3450 s). Monoclonal anti-PSD95 (Millipore, MAB1596). Anti-rabbit-IgG-CF568 (Sigma, SAB4600310). Polyclonal anti-HaloTag (Promega, G928A). Anti-HA (BioLegend, 901502). Polyclonal anti-Homer1 (Synaptic Systems, 160 006). STAR RED (Abberior, STRED), STAR ORANGE (Abberior, STORANGE), and STAR 460L (Abberior, ST460L). All antibodies were used at a dilution of 1:500.

### Quantification, statistical analysis, and reproducibility

Quantification for imaging experiments was carried out on raw fluorescent images using ImageJ to measure pixel intensities unless indicated in specific methods section. Background values estimated by pixel intensities in regions with no detectable signal were routinely subtracted. Unless otherwise noted, sample sizes were from a minimum of 3 independent animals or culture preparations. No statistical methods were used to pre-determine sample sizes in this study. Statistical analysis was conducted using GraphPad Prism 9.0 software. To compare two populations, we used unpaired or paired two-tailed Student's t-tests, as appropriate. For comparisons of 3 or more populations, we used 1-way ANOVAs with Tukey's or Dunnett's multiple comparisons tests. For all statistical analyses, p-values < 0.05 were considered significant. All data contain at least 3 biological replicates (N= independent animal or culture) except where otherwise noted in the figure legends. All other definitions of n values, statistical tests, and p values can be found in corresponding figure legends.

## Additional Resources

### R-mAb amino acid sequences

**A1 scFv-HaloTag.** METDTLLLVWLLLWVPGSTGDEVKLLSEGGGLVQPG  
GSLKLSAASGDFSEYWMWVRQAPGKGLEWIGEINPDSSSIDYTPSLKD  
KIIISRDNAKKTLYLQLSKVRSEDTALYYCARPRGNVYVMDYWGQTSVT  
VSSGGGGSGGGGGSGGGGNIVLTQSPASLAVSLGQRATISCRASESVDSYG  
SSFVHWYQKPKQGPPLKLLIFASKLESQVPAFSGSGSRTDFLTIDPVEAD  
DAATYYCQQTNEPYTFGGGKLEIKRASNGGGGGTGSAGAEIGTFPFDP  
PHYVEVLGERMHYVDVGRDGTPLVFLHGNPTSSYVWRNIIPHVAPTHRC  
IAPDLIGMGKSDKPDLYFFDDHVRFMDFIEALGLEEVVLVIHDWGSALG  
FHWAKRNPVRVKGIAFMFIRPIPTWDEWPEFARETFAFRITTDVGRKLII  
DQNVFIEGTLPMGVVRPLTEVEMDHYREPFLNPVDREPLWRFPNELPIAGE  
PANIVALVEEYMDWLHQSPVPKLLFWGTPGVLIIPPAEAARLAKSLPNCKAV  
DIGPGLNLLQEDNPDIGSEIARWLSTLEISG

**A2 Fab HC-HaloTag.** METDTLLLVWLLLWVPGSTGDMQAQLKESGPGL  
VAPSQSLITCTVSGFSLTNYGVHWVRQPPGKGLEWLGVWAGGSTNYNS  
ALMSRVSISKDNSKSVFLKMNSLQTDVTMYCAREDYDWDHFDVW  
GAGTTVTSSAKTTPPSVYPLAPGSAQTNSMVTLGCLVKGYFPEPVTVT  
WNSGSLSSGVHTFPAVLQSDLYLSSSVTPSSTWPSSETVTCNVAHPASST  
KVDDKLEVLFFQPGSGSADTITIRGYVRDNRSAGSAGSAGAEIGTFPFDP  
HYVEVLGERMHYVDVGRDGTPLVFLHGNPTSSYVWRNIIPHVAPTHRCI  
APDLIGMGKSDKPDLYFFDDHVRFMDFIEALGLEEVVLVIHDWGSALG  
FHWAKRNPVRVKGIAFMFIRPIPTWDEWPEFARETFAFRITTDVGRKLII  
DQNVFIEGTLPMGVVRPLTEVEMDHYREPFLNPVDREPLWRFPNELPIAGE  
PANIVALVEEYMDWLHQSPVPKLLFWGTPGVLIIPPAEAARLAKSLPNCKAV  
DIGPGLNLLQEDNPDIGSEIARWLSTLEISG

**A2 Fab LC.** METDTLLLVWLLLWVPGSTGDMEIQTQTSSLSASLGDRV  
TISCRASQDISNYLSWYQKPDGTVKLLIYYSRLHSGVPSRFSGSGSGIDY  
SLTINNLEQEDFATYFCQQGNTLPLTFGAGTKLELKRADAAPTISIFPPSSE  
QLTSGGASVVCFLNNFYPKDINVKWKIDGSEQRNGVLNSWTDQDSKST  
YSMSSTLTLTCKEYERHNSYTCEATHKTSTSPVKSFNNECSN

**A2 scFv-HaloTag.** METDTLLLVWLLLWVPGSTGDQAQLKESGPGLVAPS  
QSLITCTVSGFSLTNYGVHWVRQPPGKGLEWLGVWAGGSTNYNSALM  
SRVSISKDNSKSVFLKMNSLQTDVTMYCAREDYDWDHFDVWGAG  
TTVTSSGGGGSGGGGGSGGGSEIQTQTSSLSASLGDRVTISCRASQ  
DISNYLSWYQKPDGTVKLLIYYSRLHSGVPSRFSGSGSGIDYSLTINN  
LEQEDFATYFCQQGNTLPLTFGAGTKLELGGGGGLVPRGSTGAEIGTFP  
FDPHYVEVLGERMHYVDVGRDGTPLVFLHGNPTSSYVWRNIIPHVAP  
THRCIAPDLIGMGKSDKPDLYFFDDHVRFMDFIEALGLEEVVLVIHDW  
GALGFHWAKRNPVRVKGIAFMFIRPIPTWDEWPEFARETFAFRITTDV  
GRKLIIQNVFIEGTLPMGVVRPLTEVEMDHYREPFLNPVDREPLWRFP  
NELPIAGEPANIVALVEEYMDWLHQSPVPKLLFWGTPGVLIIPPAEAAR  
LAKSLPNCKAVDIGPGLNLLQEDNPDIGSEIARWLSTLEISGSGGGG  
SLEVLFQPGSGGGGGLNDIFEAKIEWHEHHHHHHH

## Reporting summary

Further information on research design is available in the Nature Portfolio Reporting Summary linked to this article.

## Data availability

All data needed to evaluate the conclusions in the paper are present in the paper and Supplementary Information. Source data are provided with this paper.

## References

- Willems, J. et al. ORANGE: A CRISPR/Cas9-based genome editing toolbox for epitope tagging of endogenous proteins in neurons. *PLOS Biol.* **18**, e3000665 (2020).
- Mikuni, T., Nishiyama, J., Sun, Y., Kamasawa, N. & Yasuda, R. High Throughput, High Resolution Mapping of Protein Localization in Mammalian Brain by In Vivo Genome Editing. *Cell* **165**, 1803–1817 (2016).
- Suzuki, K. et al. In vivo genome editing via CRISPR/Cas9 mediated homology-independent targeted integration. *Nature* **540**, 144–149 (2016).
- Gao, Y. et al. Plug-and-Play Protein Modification Using Homology-Independent Universal Genome Engineering. *Neuron* **103**, 583–597.e8 (2019).
- Fang, H., Bygrave, A. M., Roth, R. H., Johnson, R. C. & Haganir, R. L. An optimized CRISPR/Cas9 approach for precise genome editing in neurons. *eLife* **10**, e65202 (2021).
- Gross, G. G. et al. Recombinant Probes for Visualizing Endogenous Synaptic Proteins in Living Neurons. *Neuron* **78**, 971–985 (2013).
- Gross, G. G. et al. An E3 ligase-based method for ablating inhibitory synapses. *Nat. Methods* **13**, 673–678 (2016).
- Mora, R. J., Roberts, R. W. & Arnold, D. B. Recombinant Probes Reveal Dynamic Localization of CaMKII $\alpha$  within Somata of Cortical Neurons. *J. Neurosci.* **33**, 14579–14590 (2013).
- Rothbauer, U. et al. Targeting and tracing antigens in live cells with fluorescent nanobodies. *Nat. Methods* **3**, 887–889 (2006).
- Ries, J., Kaplan, C., Platonova, E., Eghlidi, H. & Ewers, H. A simple, versatile method for GFP-based super-resolution microscopy via nanobodies. *Nat. Methods* **9**, 582–584 (2012).
- Trimmer, J. S. Genetically Encoded Intrabodies As High-Precision Tools To Visualize And Manipulate Neuronal Function. *Semin Cell Dev. Biol.* **126**, 117–124 (2022).
- Dong, J.-X. et al. A toolbox of nanobodies developed and validated for use as intrabodies and nanoscale immunolabels in mammalian brain neurons. *Elife* **8**, e48750 (2019).
- Mitchell, K. G. et al. High-volume hybridoma sequencing on the NeuroMabSeq platform enables efficient generation of recombinant monoclonal antibodies and scFvs for neuroscience research. *Sci. Rep.* **13**, 16200 (2023).
- Zhao, Y., Chen, S., Swensen, A. C., Qian, W.-J. & Gouaux, E. Architecture and subunit arrangement of native AMPA receptors elucidated by cryo-EM. *Science* **364**, 355–362 (2019).
- Los, G. V. et al. HaloTag: a novel protein labeling technology for cell imaging and protein analysis. *ACS Chem. Biol.* **3**, 373–382 (2008).
- Grimm, J. B., Brown, T. A., English, B. P., Lionnet, T. & Lavis, L. D. Synthesis of Janelia Fluor HaloTag and SNAP-Tag Ligands and Their Use in Cellular Imaging Experiments. in *Super-Resolution Microscopy: Methods and Protocols* (ed. Erfle, H.) 179–188 (Springer, New York, NY, 2017).
- Grimm, J. B. et al. A general method to optimize and functionalize red-shifted rhodamine dyes. *Nat. Methods* **17**, 815–821 (2020).
- Hansen, K. B. et al. Structure, Function, and Pharmacology of Glutamate Receptor Ion Channels. *Pharm. Rev.* **73**, 298–487 (2021).
- Lu, W. et al. Subunit composition of synaptic AMPA receptors revealed by a single-cell genetic approach. *Neuron* **62**, 254–268 (2009).
- Wenthold, R. J., Petralia, R. S., J. I. B. & Niedzielski, A. S. Evidence for multiple AMPA receptor complexes in hippocampal CA1/CA2 neurons. *J. Neurosci.* **16**, 1982 (1996).
- Heine, M. et al. Surface Mobility of Postsynaptic AMPARs Tunes Synaptic Transmission. *Science* **320**, 201–205 (2008).
- Penn, A. C. et al. Hippocampal LTP and contextual learning require surface diffusion of AMPA receptors. *Nature* **549**, 384–388 (2017).
- Han, X. et al. Multiplexed volumetric CLEM enabled by scFvs provides insights into the cytology of cerebellar cortex. *Nat. Commun.* **15**, 6648 (2024).
- Hunker, A. C. et al. Conditional Single Vector CRISPR/SaCas9 Viruses for Efficient Mutagenesis in the Adult Mouse Nervous System. *Cell Rep.* **30**, 4303–4316.e6 (2020).
- Kennedy, M. J., Davison, I. G., Robinson, C. G. & Ehlers, M. D. Syntaxin-4 Defines a Domain for Activity-Dependent Exocytosis in Dendritic Spines. *Cell* **141**, 524–535 (2010).

26. Hiester, B. G. et al. L-Type Voltage-Gated Ca<sup>2+</sup> Channels Regulate Synaptic Activity-Triggered Recycling Endosome Fusion in Neuronal Dendrites. *Cell Rep.* **21**, 2134–2146 (2017).
27. Makino, H. & Malinow, R. AMPA receptor incorporation into synapses during LTP: the role of lateral movement and exocytosis. *Neuron* **64**, 381–390 (2009).
28. Getz, A. M. et al. High-resolution imaging and manipulation of endogenous AMPA receptor surface mobility during synaptic plasticity and learning. *Sci. Adv.* **8**, eabm5298 (2022).
29. Hiester, B. G., Becker, M. I., Bowen, A. B., Schwartz, S. L. & Kennedy, M. J. Mechanisms and Role of Dendritic Membrane Trafficking for Long-Term Potentiation. *Front. Cell Neurosci.* **12**, (2018).
30. Lu, W.-Y. et al. Activation of Synaptic NMDA Receptors Induces Membrane Insertion of New AMPA Receptors and LTP in Cultured Hippocampal Neurons. *Neuron* **29**, 243–254 (2001).
31. Ehlers, M. D. Reinsertion or Degradation of AMPA Receptors Determined by Activity-Dependent Endocytic Sorting. *Neuron* **28**, 511–525 (2000).
32. Boucher, L. E. et al. “Stapling” scFv for multispecific biotherapeutics of superior properties. *MAbs* **15**, 2195517 (2023).
33. Andrews, N. P. et al. A toolbox of IgG subclass-switched recombinant monoclonal antibodies for enhanced multiplex immunolabeling of brain. *eLife* **8**, e43322 (2019).
34. O’Brien, R. J. et al. Activity-Dependent Modulation of Synaptic AMPA Receptor Accumulation. *Neuron* **21**, 1067–1078 (1998).
35. Turrigiano, G. G., Leslie, K. R., Desai, N. S., Rutherford, L. C. & Nelson, S. B. Activity-dependent scaling of quantal amplitude in neocortical neurons. *Nature* **391**, 892–896 (1998).
36. Sutton, M. A. & Schuman, E. M. Local translational control in dendrites and its role in long-term synaptic plasticity. *J. Neurobiol.* **64**, 116–131 (2005).
37. Lee, S. H. et al. Super-resolution imaging of synaptic and Extrasynaptic AMPA receptors with different-sized fluorescent probes. *eLife* **6**, e27744 (2017).
38. Sinnen, B. L. et al. Optogenetic control of synaptic composition and function. *Neuron* **93**, 646–660.e5 (2017).
39. Hangen, E., Cordelières, F. P., Petersen, J. D., Choquet, D. & Cousen, F. Neuronal Activity and Intracellular Calcium Levels Regulate Intracellular Transport of Newly Synthesized AMPAR. *Cell Rep.* **24**, 1001–1012.e3 (2018).
40. Bowen, A. B., Bourke, A. M., Hiester, B. G., Hanus, C. & Kennedy, M. J. Golgi-independent secretory trafficking through recycling endosomes in neuronal dendrites and spines. *eLife* **6**, e27362 (2017).
41. Bourke, A. M. et al. zapERtrap: A light-regulated ER release system reveals unexpected neuronal trafficking pathways. *J. Cell Biol.* **220**, e202103186 (2021).
42. Al-Bassam, S., Xu, M., Wandless, T. J. & Arnold, D. B. Differential trafficking of transport vesicles contributes to the localization of dendritic proteins. *Cell Rep.* **2**, 89–100 (2012).
43. Bourke, A. M. & Kennedy, M. J. Spatial and Temporal Control of Protein Secretion with Light. in *Membrane Trafficking: Methods and Protocols* (ed. Shen, J.) 29–45 (Springer US, New York, NY, 2022).
44. Zhang, C. et al. Suppression of p75 Neurotrophin Receptor Surface Expression with Intrabodies Influences Bcl-xL mRNA Expression and Neurite Outgrowth in PC12 Cells. *PLoS One* **7**, e30684 (2012).
45. Strebe, N. et al. Functional knockdown of VCAM-1 at the post-translational level with ER retained antibodies. *J. Immunol. Methods* **341**, 30–40 (2009).
46. Liu, Q. et al. A Photoactivatable Botulinum Neurotoxin for Inducible Control of Neurotransmission. *Neuron* **101**, 863–875.e6 (2019).
47. Shi, S.-H., Hayashi, Y., Esteban, J. A. & Malinow, R. Subunit-Specific Rules Governing AMPA Receptor Trafficking to Synapses in Hippocampal Pyramidal Neurons. *Cell* **105**, 331–343 (2001).
48. Díaz-Alonso, J. et al. Subunit-specific role for the amino-terminal domain of AMPA receptors in synaptic targeting. *Proc. Natl Acad. Sci. USA* **114**, 7136–7141 (2017).
49. Watson, J. F., Ho, H. & Greger, I. H. Synaptic transmission and plasticity require AMPA receptor anchoring via its N-terminal domain. *eLife* **6**, e23024 (2017).
50. Incontro, S., Asensio, C. S., Edwards, R. H. & Nicoll, R. A. Efficient, Complete Deletion of Synaptic Proteins using CRISPR. *Neuron* **83**, 1051–1057 (2014).
51. Straub, C., Granger, A. J., Saulnier, J. L. & Sabatini, B. L. CRISPR/Cas9-Mediated Gene Knock-Down in Post-Mitotic Neurons. *PLoS One* **9**, e105584 (2014).
52. Archibald, K., Perry, M. J., Molnár, E. & Henley, J. M. Surface expression and metabolic half-life of AMPA receptors in cultured rat cerebellar granule cells. *Neuropharmacology* **37**, 1345–1353 (1998).
53. Chen, D., Gibson, E. S. & Kennedy, M. J. A light-triggered protein secretion system. *J. Cell Biol.* **201**, 631–640 (2013).
54. Levy, J. M., Chen, X., Reese, T. S. & Nicoll, R. A. Synaptic Consolidation Normalizes AMPAR Quantal Size following MAGUK Loss. *Neuron* **87**, 534–548 (2015).
55. Zhao, N. et al. A genetically encoded probe for imaging nascent and mature HA-tagged proteins in vivo. *Nat. Commun.* **10**, 2947 (2019).
56. Beaudoin, G. M. J. et al. Culturing pyramidal neurons from the early postnatal mouse hippocampus and cortex. *Nat. Protoc.* **7**, 1741–1754 (2012).
57. Concordet, J.-P. & Haeussler, M. CRISPOR: intuitive guide selection for CRISPR/Cas9 genome editing experiments and screens. *Nucleic Acids Res* **46**, W242–W245 (2018).
58. O’Brien, R. J. et al. The development of excitatory synapses in cultured spinal neurons. *J. Neurosci.* **17**, 7339–7350 (1997).
59. Chen, T.-W. et al. Ultrasensitive fluorescent proteins for imaging neuronal activity. *Nature* **499**, 295–300 (2013).
60. Rizk, A. et al. Segmentation and quantification of subcellular structures in fluorescence microscopy images using Squash. *Nat. Protoc.* **9**, 586–596 (2014).
61. Bolte, S. & Cordelières, F. P. A guided tour into subcellular colocalization analysis in light microscopy. *J. Microsc.* **224**, 213–232 (2006).

## Acknowledgements

The authors would like to thank members of the Kennedy lab for critical discussions. Super resolution imaging was performed at the University of Colorado Anschutz Medical Campus Advanced Light Microscopy Core. This work was supported by F32 MH123053 (S.S.O.); F31NS130979 (D.J.K.); F30DA057053 (C.N.M.); R01MH116901 (J.A.); R35NS116879, R21MH134019, R01MH134957 (M.J.K.).

## Author contributions

M.J.K. designed and supervised the project. A1 scFv-Halo, A2 Fab-Halo, and A2 scFv-Halo were designed by M.J.K. and cloned by C.S.W. and D.J.K. CRISPR/Cas9 validation of A1 and A2 parent R-mAbs was performed by M.J.K. and C.S.W. A1 scFv-Halo was designed and cloned by D.J.K. FRAP comparing A2 Fab-Halo, A2 scFv-Halo, and A1 scFv-Halo mobility was performed by A.M.R., D.J.K., and M.J.K. Recording mEPSCs from cultured hippocampal neurons following acute application of A1 scFv-Halo and A2 Fab-Halo was performed by C.A.K. and D.J.K., respectively. Optical quantal R-mAb experiments were carried out by H.S.A. Experiments assessing total GluA1 levels in cells expressing A1 scFv-KDEL or A2 scFv-KDEL and analyses were carried out by H.J.R. and D.J.K., respectively. All other STED acquisitions and analyses were performed by S.S.O. Stereotaxic injection of all mice was performed and C.A.K. and by J.K., supervised by J.A. Acute slice LTP experiments were designed by J.A. and performed by D.J.K. and C.M. under supervision of J.A. All other experiments and analyses were performed by D.J.K. The

figures were prepared by D.J.K. The manuscript was written by D.J.K. and M.J.K. All authors read and edited the paper.

## Competing interests

The authors declare no competing interests.

## Additional information

**Supplementary information** The online version contains supplementary material available at <https://doi.org/10.1038/s41467-024-54530-5>.

**Correspondence** and requests for materials should be addressed to Matthew J. Kennedy.

**Peer review information** *Nature Communications* thanks the anonymous reviewers for their contribution to the peer review of this work. A peer review file is available.

**Reprints and permissions information** is available at <http://www.nature.com/reprints>

**Publisher's note** Springer Nature remains neutral with regard to jurisdictional claims in published maps and institutional affiliations.

**Open Access** This article is licensed under a Creative Commons Attribution-NonCommercial-NoDerivatives 4.0 International License, which permits any non-commercial use, sharing, distribution and reproduction in any medium or format, as long as you give appropriate credit to the original author(s) and the source, provide a link to the Creative Commons licence, and indicate if you modified the licensed material. You do not have permission under this licence to share adapted material derived from this article or parts of it. The images or other third party material in this article are included in the article's Creative Commons licence, unless indicated otherwise in a credit line to the material. If material is not included in the article's Creative Commons licence and your intended use is not permitted by statutory regulation or exceeds the permitted use, you will need to obtain permission directly from the copyright holder. To view a copy of this licence, visit <http://creativecommons.org/licenses/by-nc-nd/4.0/>.

© The Author(s) 2024